

EFFECTS OF TYPES OF ARYLAMINE BASED BENZOXAZINE BINDERS IN BRAKE PADS ON
THERMAL DEGRADATION KINETICS



A Thesis Submitted in Partial Fulfillment of the Requirements
for the Degree of Master of Engineering in Chemical Engineering

Department of Chemical Engineering

FACULTY OF ENGINEERING

Chulalongkorn University

Academic Year 2021

Copyright of Chulalongkorn University

ผลของชนิดตัวยัดเกาะเบนชอกซาซีนที่มีหมู่เอริลลามีนต่างกันในตัวเบรกต่อจลนพลศาสตร์การ
สลายตัวทางความร้อน



วิทยานิพนธ์นี้เป็นส่วนหนึ่งของการศึกษาตามหลักสูตรปริญญาวิศวกรรมศาสตรมหาบัณฑิต
สาขาวิชาวิศวกรรมเคมี ภาควิชาวิศวกรรมเคมี
คณะวิศวกรรมศาสตร์ จุฬาลงกรณ์มหาวิทยาลัย
ปีการศึกษา 2564
ลิขสิทธิ์ของจุฬาลงกรณ์มหาวิทยาลัย

Thesis Title	EFFECTS OF TYPES OF ARYLAMINE BASED BENZOXAZINE BINDERS IN BRAKE PADS ON THERMAL DEGRADATION KINETICS
By	Mr. Juntasak Wangrangsimakul
Field of Study	Chemical Engineering
Thesis Advisor	VARUN TAEPAISITPHONGSE, Ph.D.
Thesis Co Advisor	Professor SARAWUT RIMDUSIT, Ph.D.

Accepted by the FACULTY OF ENGINEERING, Chulalongkorn University in Partial Fulfillment of the Requirement for the Master of Engineering

..... Dean of the FACULTY OF ENGINEERING
(Professor SUPOT TEACHAVORASINSKUN, D.Eng.)

THESIS COMMITTEE

..... Chairman
(Assistant Professor AMORNCHAI ARPORNWICHANOP, D.Eng.)

..... Thesis Advisor
(VARUN TAEPAISITPHONGSE, Ph.D.)

..... Thesis Co-Advisor
(Professor SARAWUT RIMDUSIT, Ph.D.)

..... Examiner
(Professor MUENDUEN PHISALAPHONG, Ph.D.)

..... External Examiner
(Associate Professor Chanchira Jubsilp, D.Eng.)

จันทศักดิ์ หวังรังสีมากุล : ผลของชนิดตัวยึดเกาะเบนซอกซาซีนที่มีหมู่เอริลลามีนต่างกัน
ในผ้าเบรกต่อจลนพลศาสตร์การสลายตัวทางความร้อน. (EFFECTS OF TYPES OF
ARYLAMINE BASED BENZOXAZINE BINDERS IN BRAKE PADS ON THERMAL
DEGRADATION KINETICS) อ.ที่ปรึกษาหลัก : ดร.วรัญ แต่ไพสิฐพงษ์, อ.ที่ปรึกษาร่วม :
ศ. ดร.ศราวุธ ริมดุสิต

งานวิจัยนี้มีจุดมุ่งหมายเพื่อศึกษาอิทธิพลของหมู่เอริลลามีนบนตัวยึดเกาะพอลิเบนซอกซาซีน ที่มีต่อการสลายตัวและเสถียรภาพทางความร้อนของผ้าเบรกชนิดปราศจากแร่ใยหิน โดยทำการศึกษาการสลายตัวทางความร้อนของวัสดุคอมโพสิตที่มีพอลิเบนซอกซาซีนชนิด 3,5-ไซลิดีนเป็นส่วนผสมในตัวยึดเกาะของผ้าเบรก โดยการวิเคราะห์หาค่าพารามิเตอร์ทางจลนพลศาสตร์ ได้แก่ ค่าพลังงานก่อกัมมันต์และกลไกการเกิดปฏิกิริยาการสลายตัวทางความร้อนด้วยเครื่อง Thermogravimetric Analysis (TGA) ในบรรยากาศไนโตรเจน ที่อัตราการให้ความร้อน 1, 5, 10, 20 และ 25 องศาเซลเซียสต่อนาที โดยใช้โมเดลของ advanced iso-conversional method จากการวิเคราะห์การสลายตัวทางความร้อนของชิ้นงานพบว่า การสลายตัวทางความร้อนของวัสดุคอมโพสิตของพอลิเบนซอกซาซีนประกอบไปด้วยขั้นตอนการเกิดปฏิกิริยาหลัก 6 ขั้นตอน โดยค่าพลังงานก่อกัมมันต์ ซึ่งได้จากการวิเคราะห์ด้วยวิธี Kissinger, Flynn-Wall-Ozawa และ วิธี Coats-Redfern ของการสลายตัวทางความร้อนทั้ง 6 ขั้นตอน มีค่าเฉลี่ยประมาณ 244, 286, 224, 108, 357 และ 526 กิโลจูลต่อโมล ตามลำดับ นอกจากนี้จากการวิเคราะห์ด้วยวิธีจลนพลศาสตร์ Criado method จะได้ว่า กลไกปฏิกิริยาการสลายตัวทางความร้อนในแต่ละขั้นตอนของชิ้นงานผ้าเบรก มีรูปแบบการสลายตัวทางความร้อนเป็นแบบการสุ่มสลายตัวของแต่ละนิวเคลียสในแต่ละอนุภาค (random nucleation with one nucleus on the individual particle, F1)

สาขาวิชา วิศวกรรมเคมี
ปีการศึกษา 2564

ลายมือชื่อนิสิต
ลายมือชื่อ อ.ที่ปรึกษาหลัก
ลายมือชื่อ อ.ที่ปรึกษาร่วม

6070914821 : MAJOR CHEMICAL ENGINEERING

KEYWORD: Friction Composite Materials, Thermal Stability, Polybenzoxazine,
Degradation Kinetics

Juntasak Wangrangsimakul : EFFECTS OF TYPES OF ARYLAMINE BASED
BENZOXAZINE BINDERS IN BRAKE PADS ON THERMAL DEGRADATION
KINETICS. Advisor: VARUN TAEPAISITPHONGSE, Ph.D. Co-advisor: Prof.
SARAWUT RIMDUSIT, Ph.D.

This research aimed to investigate the effect of the alkyl-substituted aromatic amines of polybenzoxazine resins used as binders in the non-asbestos friction composite materials on their thermal degradation and stability. The effects of BA-35x polybenzoxazine resin used as a binder of the brake pad were investigated using thermogravimetric analysis (TGA) under nitrogen atmosphere at various heating rates of 1, 5, 10, 20 and 25 °C/min by applying the model of Advanced iso-conversional method. For the friction composite system using BA-35x as binder, the derivative thermogram exhibited six stages of thermal decomposition reaction. The activation energies of six stages were determined by Kissinger method, Flynn-Wall-Ozawa method and Coats-Redfern method to be 244, 286, 224, 108, 357 and 526 kJ/mol, respectively. Furthermore, from the calculation by Criado method, the thermal degradation mechanism was proposed to be the appropriated type of random nucleation with one nucleus on the individual particle (F1).

Field of Study: Chemical Engineering

Academic Year: 2021

Student's Signature

Advisor's Signature

Co-advisor's Signature

ACKNOWLEDGEMENTS

The author would like to express sincere gratitude to my advisors, Dr. Varun Taepaisitphongse and Prof. Dr. Sarawut Rimdusit, for their vision, suggestion, and advice with kindness in the course of this study. Furthermore, I would like to thank all thesis committee: Asst. Prof. Dr. Amornchai Arpornwichanop, Prof. Dr. Muenduen Phisalaphong, and Assoc. Prof. Dr. Chanchira Jubsilp for the kind guide and good comments.

Additionally, I would like to thank all my colleagues in the Polymer Engineering Laboratory, Chulalongkorn University, for their discussions and friendly encouragement. Finally, I would like to thank, from the bottom of my heart, my parents who always give their unfailing love, understanding, and generous encouragement throughout my entire study.

Juntasak Wangrangsimakul

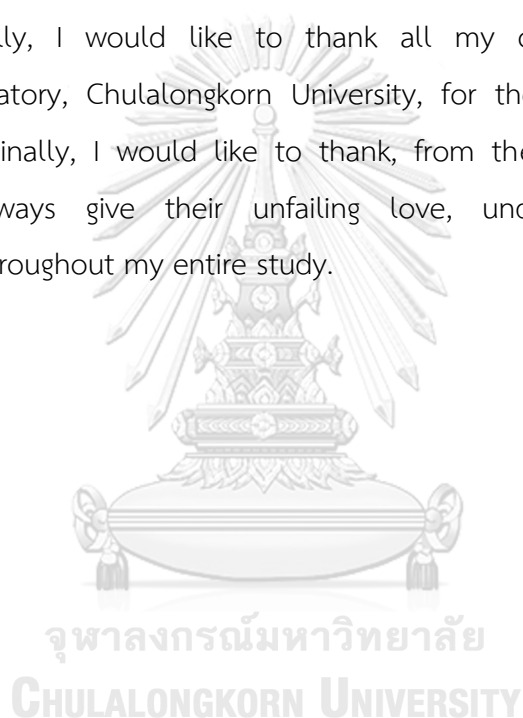


TABLE OF CONTENTS

	Page
ABSTRACT (THAI).....	iii
ABSTRACT (ENGLISH).....	iv
ACKNOWLEDGEMENTS.....	v
TABLE OF CONTENTS.....	vi
LIST OF TABLES.....	viii
LIST OF FIGURES.....	ix
CHAPTER I INTRODUCTION.....	1
1.1 General Introduction.....	1
1.2 Objectives.....	4
1.3 Scopes of the Study.....	4
CHAPTER II THEORY.....	5
2.1 Friction Materials.....	5
2.2 Benzoxazine Resin.....	11
2.3 Kinetics of Polymer Degradation.....	16
2.4 Deconvolution Method.....	23
CHAPTER III LITERATURE REVIEWS.....	24
CHAPTER IV EXPERIMENTAL.....	29
4.1 Raw Materials.....	29
4.2 Preparation of Benzoxazine Resin.....	29
4.3 Synthesis of Compositated Friction Material.....	30
4.4 Sample Characterization.....	31

CHAPTER V RESULTS AND DISCUSSION.....	33
5.1 Effects of Types of Arylamines Based Benzoxazine Binder on Thermal Stability of Brake Pad Composites.....	33
5.2 Analysis of Thermal Degradation Kinetic of Friction Composite.....	38
5.3 Determination of Thermal Degradation Kinetic Parameters.....	40
5.4 Thermal Degradation Mechanism of the Brake Pad Composites.....	50
CHAPTER VI CONCLUSIONS.....	53
APPENDIX A Arylamine-based Benzoxazine Resins Properties.....	54
APPENDIX B Arylamine-based Benzoxazine Composite Properties.....	55
APPENDIX C Thermal Properties of Some Friction Composite Ingredients.....	57
APPENDIX D Thermal Data for Kinetics Analysis.....	58
APPENDIX E Kinetic Parameters Reported in Literature.....	77
REFERENCES.....	78
VITA.....	86

LIST OF TABLES

	Page
Table 1 Type of Binders for Automotive Brake Friction Materials	8
Table 2 Common Fillers Used in Friction Materials.....	9
Table 3 Reinforcing Fiber Types Used in Friction Materials.....	10
Table 4 Types of Friction Additives for Friction Materials.....	11
Table 5 Thermal Properties of Arylamine-Based Polybenzoxazines.....	14
Table 6 Algebraic Expressions for $g(\alpha)$ and $f(\alpha)$ for the Most Frequently Used Mechanisms of Solid-State Processes	22
Table 7 Thermal Properties of Binders.....	25
Table 8 Formulation of Polybenzoxazine Composite Friction Material	30
Table 9 Weight Loss Data and Char Yield from Thermal Decomposition in Nitrogen Atmosphere	34
Table 10 Storage Modulus and Crosslink Density of Polybenzoxazine Composite Friction Materials.....	37
Table 11 Activation Energies Determined by Kissinger Method for BA-35x Based Friction Composite from Different Heating Rates	41
Table 12 Activation Energies Obtained by Using Flynn-Wall-Ozawa Method for BA-35x Based Friction Composite at Various Conversions.....	44

LIST OF FIGURES

	Page
Figure 1 Types of Brakes; (a) Drum Brake, (b) Disc Brake.....	5
Figure 2 Sketch of Drum Brake and its Components	6
Figure 3 Sketch of Disc Brakes and their Assembles: (a) Sliding Disc Brake, (b) Fixed Disc Brake	7
Figure 4 Various Types of Benzoxazine Monomer: (a) 3-Methyl-2H, 4H-Benzo[e]1,3-oxazine, (b) 1-Methyl-2H,4H-Benzo[d]1,3-oxazine, (c) 4-Methyl-2H,3H-Benzo[e]1,4-oxazine, and (d) 2H-Benzo[e]1,3-oxazine.....	11
Figure 5 Synthesis of an Aniline Based Benzoxazine Resin (BA-a).....	12
Figure 6 Synthesis of a Bifunctional Benzoxazine Monomer.....	13
Figure 7 Polymerization of Benzoxazines	13
Figure 8 Benzoxazine Resins from Different Alkyl-Substituted Aromatic Amines: (a) 6,69-Bis(3-(2-Methyl) Phenyl-3,4-Dihydro-2H-1,3-Benzoxazinyl) Isopropane (BA-ot), (b) 6,69-Bis(3-(4-Methyl) Phenyl-3,4-Dihydro-2H-1,3-Benzoxazinyl) Isopropane (BA-pt), (c) 6,69-Bis(3-Phenyl-3,4-Dihydro-2H-1,3-Benzoxazinyl) Isopropane (BA-a), (d) 6,69-Bis (3-(3-Methyl)-Phenyl-3,4-Dihydro-2H-1,3-Benzoxazinyl) Isopropane (BA-mt), (e) 6,69- Bis(3-(3,5-Dimethyl)Phenyl-3,4-Dihydro-2H-1,3-Benzoxazinyl) Isopropane (BA-35x)	15
Figure 9 The Phenolic Mannich Bridge Network Formation	25
Figure 10 The Arylamine Mannich Bridge Network Formation.....	26
Figure 11 Proposed Degradation Process of Mannich Base Cleavage in Benzoxazine Dimer.....	27
Figure 12 Polymerization of Benzoxazines Monomer BA-a	30
Figure 13 Thermal Gravimetric Analyzer (TGA): Model TGA1 STARe from Mettler-Toledo.....	31

- Figure 14 TGA Thermogram from Degradation of Polybenzoxazine and Friction Composites Prepared from Different Benzoxazine Resin: (X) BA-ot Polybenzoxazine, (*) BA-pt Polybenzoxazine, (●) PBA-a Polybenzoxazine, (◇) BA-mt Polybenzoxazine, (■) BA-35x Polybenzoxazine, (▲) BA-ot based Friction Composite, (◆) BA-pt based Friction Composite, (Δ) BA-a based Friction Composite, (□) BA-mt based Friction Composite, (O) BA-35x based Friction Composite 33
- Figure 15 Derivative TGA Thermogram of BA-35x Brake Pad Composite and Its Separated Peaks by Using Simulation Software: (●) Experimental Data, (—) Simulated Curve (heating rate 20 °C/min) 39
- Figure 16 The Relation between $\ln(\beta/T_p^2)$ and $1000/T_p$ as per Kissinger Method (●) Peak 1, (▲) Peak 2, (◆) Peak 3, (■) Peak 4, (O) Peak 5, (Δ) Peak 6 41
- Figure 17 The Relation between $\log \beta$ versus $1000/T$ according to Flynn-Wall-Ozawa Method for BA-35x friction Composite for (a) Peak 1, (b) Peak 2, (c) Peak 3, (d) Peak 4, (e) Peak 5, and (f) Peak 6, with Conversion of (●) 10%, (▲) 20%, (■) 40%, (◆) 60%, (X) 80%, and (Δ) 100%. 43
- Figure 18 The Relation between $\ln(g(\alpha)/T^2)$ versus $1000/T$ according to Coat-Redfern Method for BA-35x Brake Pad Composites For Various Reaction Mechanism at The Heating Rate of 20 °C/min for (a) Peak 1, (b) Peak 2, (c) Peak 3, (d) Peak 4, (e) Peak 5, (f) Peak 6, and Reaction Mechanism for (◆) A2, (O) A3, (▲) A4, (X) R1, (*) R2, (●) R3, (+) D1, (-) D2, (—) D3, (◇) D4, (■) F1, (Δ) F2, and (□) F3. 47
- Figure 19 Theoretical Plots of $Z(\alpha)$ versus α (Master Curves) and Experimental Plot According to Criado Method of The BA-35x Based Friction Composite at Different Mechanisms for (a) Peak 1, (b) Peak 2, (c) Peak 3, (d) Peak 4, (e) Peak 5, (f) Peak 6, and Reaction Mechanism for (◆) A2, (O) A3, (▲) A4, (X) R1, (*) R2, (●) R3, (+) D1, (-) D2, (—) D3, (◇) D4, (■) F1, (Δ) F2, (□) F3 and (----) Experiment 52

CHAPTER I

INTRODUCTION

1.1 General Introduction

One of the most crucial parts in all automotive applications is the braking system which includes controlled friction, wear behavior, and thermal degradation. Friction materials play an important role in the brake system since brakes use friction to stop the motion of vehicle. A conventional automotive braking system consists of a disc and brake-lining pads, and must fulfill requirements such as good wear resistance, a stable coefficient of friction, reduced noise, decreased emission of particulate matter, and proper mechanisms that affect thermal and frictional properties [1].

In the recent time, composite polymer-based friction materials have been finding greatly increased potentials for applications in several industries including automotive, self-lubricating materials, industrial equipment and aerospace. Their typical benefits include ease in manufacturing, low cost, high damping of noise and vibrations, low friction, and self-lubrication [2]. Basically, phenolic resins are polymer that consisting of several structures based on the products of phenols and formaldehydes. They have some advantages including thermal resistance, flame retardance, dielectric insulation properties; therefore they are employed in many engineering material applications [3, 4]. Though phenolic-based materials are widely used to meet several desirable properties, such as good mechanical strength, moldability, economy, high thermal and dimensional stability, resistance against various chemicals and flame retardance, a number of short-comings are also associated with these materials [5]. A typical binder in composite brake friction materials including phenolics is brittle, highly toxic, has low impact resistance, and decomposes at relatively low temperature, while brake pads and brake shoes are exposed to high compressive and shear forces [6].

Benzoxazines, a new type of phenolic resins, are developed to overcome the shortcomings of traditional phenolics while retaining their benefits. Benzoxazine resins are easily synthesized from phenol, formaldehyde, and amine by employing

solution or solventless methods [7]. The polymerization of benzoxazine resins proceeds via ring opening of oxazine rings by thermal cure. In addition, they do not require catalysts for polymerization and do not produce by-product upon curing [8]. Polybenzoxazines have emerged as superior alternative to classical phenolic resins for the past few decades [9]. These resins have structural resemblance to classical phenolics and, thus, many properties are similar. However, the tertiary amine groups in polybenzoxazines have drastic effect on the structure resulting in inter- and intramolecular hydrogen bonds between amino groups and phenolic hydroxyls which are unusual for classical phenolics [10, 11]. Accordingly, polybenzoxazines have high mechanical strength, chemical resistance against acids and bases, high char yield, high glass transition temperature (T_g), and relatively high service temperatures. Besides these important aspects, polybenzoxazines also bear in features that are uncommon for many resins such as low water adsorption that seems to be in contrast to phenolic nature but stems from intramolecular hydrogen bonds, and limited or no shrinkage upon curing due to the chain conformation of polybenzoxazines [12]. Therefore, polybenzoxazines have found various applications in industrial such as aerospace composites, electronic circuit boards, blends and alloys [10, 13].

Generally, phenolic and epoxy resins are the most common resin binders used in the composite friction materials, that is, conventional brake pads due to characteristics such as moldability, economy, chemical resistance, good mechanical properties, and flame resistance. But they still have the disadvantage for being highly toxic and decompose at relatively low temperature [10, 13]. Alkyl-substituted aromatic amines based benzoxazines, as a kind of phenolics, are high performance thermosets which possess various advantageous characteristics that overcome some drawbacks of conventional phenolic and epoxy resins such as high thermal stability, abrasion resistance, and superior tribological characteristics [7]. Although there are many studies about mechanical properties, friction and wear behaviors of the arylamine polybenzoxazine-based brake pad, little was known about the thermal degradation of these materials [14]. This research studied the effects of alkyl-substituted aromatic amines of polybenzoxazine used as binder matrix of friction

composite materials on their thermal stability and degradation. Benzoxazine resins were prepared from bisphenol-A and aromatic amines (o-toluidine, p-toluidine, aniline, m-toluidine, and 3,5-xylidine) and were used as the binder resins because they posted similar structure with just different position of the alkyl-substituted group of aromatic amines [8]. These binders that were prepared from arylamine based benzoxazine resins (BA-ot, BA-pt, BA-a, BA-mt, and BA-35x) had different thermal and mechanical properties and crosslink densities. They were also notable for high friction coefficient for all composites which could be explained by the behaviors of their storage and loss moduli of the binder matrices [10, 13]. Studying the degradation behavior of materials and relating it to degradation kinetics is an essential topic and gives ability to determine the degradation mechanisms and the stability of the material under various thermal conditions.

The thermal characteristic dataset, such as degradation temperatures and their derivatives, in this field of study were determined by Thermogravimetric analysis (TGA). These are typically the main process variables that are taken into consideration when degradation reaction kinetics are in question. The thermal degradation kinetic parameters, i.e., activation energies, were evaluated by using three well-known methods, i.e., Kissinger method, Flynn-Wall-Ozawa method, and Coats-Redfern method. Especially, Kissinger method and Flynn-Wall-Ozawa method were used in this study because these methods could yield a significantly accurate value of the activation energy regardless of the process complexity and could be applied without prior knowledge of reaction mechanisms [8]. Additionally, Coats-Redfern method was used because it rendered the degradation parameters and possible reaction mechanism. The thermal degradation mechanisms of friction composites were also evaluated by using Criado method [14].

1.2 Objectives

To investigate the effects of arylamine in benzoxazine binder on the thermal stability of brake pad and evaluate the kinetic parameters and mechanisms of the thermal degradation of polybenzoxazine composites as friction material.

1.3 Scopes of the Study

1. Synthesis of benzoxazine resins based on bisphenol-A, formaldehyde and aromatic amines (o-toluidine, p-toluidine, aniline, m-toluidine, and 3,5-xylidine) by using solventless technology.

2. Preparation of friction material composite composed of benzoxazine binder at 10 wt% and ingredients as per the following:

- Reinforcing fibers at 25 wt% iron fiber, 10 wt% glass fiber and 5 wt% aramid pulps with carbon fiber
- Friction modifiers at 25 wt% zirconium silicate and 7 wt% graphite
- Fillers at 10 wt% barium sulphate, 4 wt% rubber dust and 4 wt% cashew dusts

3. Study the effects of types of arylamines based benzoxazine binder in brake pad composites on their thermal stability.

4. Determine the thermal degradation kinetic parameters based on the methods of Kissinger, Flynn-Wall-Ozawa, and Coats-Redfern.

5. Analyze the thermal stability and degradation mechanisms of the arylamine based benzoxazine composite brake pad using Criado method.

CHAPTER II

THEORY

2.1 Friction Materials

Friction materials are used to induce friction in situations where slow or decreased movement are necessary [15]. The basic concept of any braking systems is to dissipate kinetic energy, whether in a horse drawn carriage, a car, a train, or even an aircraft; this energy is dissipated through friction due to viscosity, such as in magnetorheological brakes, or friction between sliding surfaces [16]. The type of friction to be used in a brake is determined by the application and the brake type depending on the shear stress, temperatures, dissipated power, and different materials [17]. The science that studies friction between surfaces is called tribology and was founded as a new discipline in the 1960s [18].

The most important types of brakes currently used are the so-called drum and disc brakes [16] as shown in Figure 1. The drum brake is normally fitted on the rear axle of small cars, trailers, and trucks [19]. This brake uses friction caused by a set of shoes that press outward against a rotating cylinder-shaped part called a brake



a



b

Figure 1 Types of Brakes; (a) Drum Brake, (b) Disc Brake [19].

drum. The self-energizing shoe is forced into the drum by the movement of the drum itself and is mounted so that its friction surface pushes forward of its pivot point as shown in Figure 2, while the de-energizing shoe has the opposite behavior [20]. Trailing and self-energizing action is produced by hooking the heel of the primary shoe to the toe of the secondary shoe that is located outside [19]. When the

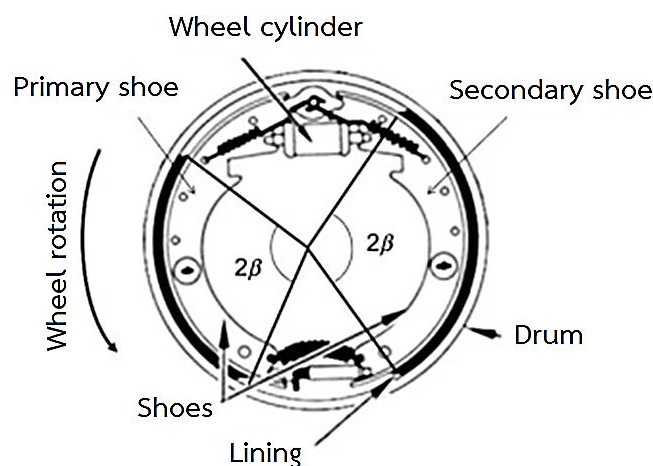


Figure 2 Sketch of Drum Brake and its Components [19].

wheel cylinder forces the top ends of the shoes against the revolving brake drum, it will try to carry the forward shoe around. As the primary shoe attempts to revolve, it will jam the secondary shoe against the single anchor pin. This stops both shoes and produces a binding effect that helps their function [16]. The purpose of this self-energizing and trailing action is to reduce the amount of needed pedal pressure [21].

The disc brake is widely used in ground vehicles, especially passenger cars [6]. However, recently the use of this type of brake has been spreading to many other kinds of ground vehicles, from bikes to heavy trucks and high-speed trains. In general, disc brakes offer better braking performances in comparison with drum brakes, since the disc is more quickly cooled [22]. The brake pads pushing against the rotors produce friction, which converts the kinetic energy into thermal energy [23]. The

sliding disc brake is shown in Figure 3 in which the pressure force is supplied by one or more pistons on the side of the caliper. The caliper itself can slide over two pins so that the braking force is also transferred to the brake pads opposite to the piston [24].

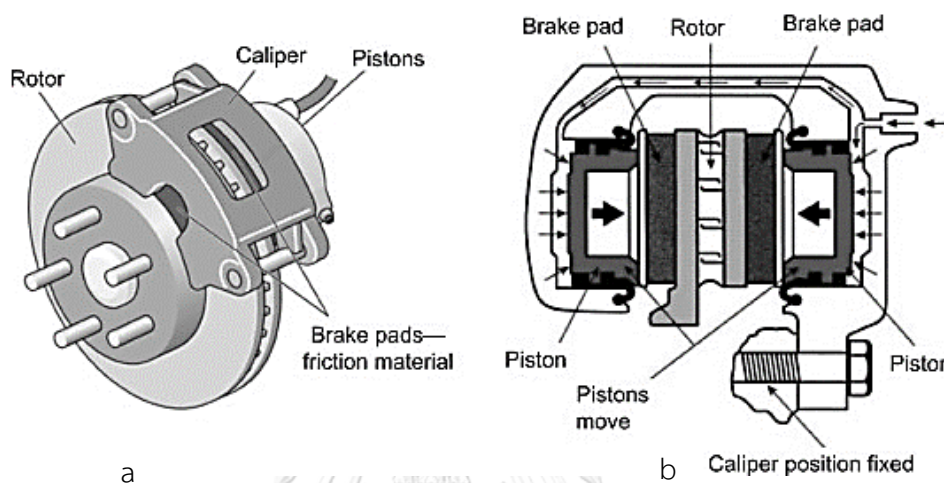


Figure 3 Sketch of Disc Brakes and their Assemblies: (a) Sliding Disc Brake, (b) Fixed Disc Brake [19].

Polymer-based friction materials are essentially multi-ingredient systems in order to achieve the desired combination of performance properties [25]. The ingredients of these composite material are categorized into four classes of ingredients including binders, reinforcement fibers, fillers, and friction modifiers [26]. The main effect of binder is to create a network that incorporates all the fillers or friction modifiers. Binder is the heart of a system which binds the ingredients firmly so that they can perform the desired function in the friction materials [26, 27]. In principle, binders, such as phenolic resin, cyanate ester resin, thermoplastic polyamide resin, are important ingredients in the brake pad materials that containing different constituents as listed in Table 1. In the past ten to twenty years, brake pad composites utilized benzoxazine resins as polymeric binders have been increasingly

developed [26]. Benzoxazine resins have distinctive advantages that are suitable for employing as polymeric binders for friction composites, including very low melt viscosity, good interfacial adhesion with fillers, self-polymerization upon heating via ring-opening polymerization without catalyst or curing agent, and no by-product release in the curing process [28].

Table 1 Type of Binders for Automotive Brake Friction Materials [6].

Binders	Advantages	Disadvantages
Phenolic resin (PF)	Cheap and easy to produce	Brittle, low-impact resistance, highly toxic, decomposes at relatively low temperature (450 °C)
COPNA resin*	High bonding strength with graphite; therefore, it has better wear resistance than pure PF	Decomposes at relatively low temperature (450–500 °C)
Silicone-modified PF	Better impact resistance than pure PF; better heat and chemical resistance than PF; enhanced water repellency	Base is still PF and highly toxic
Cyanate ester resin	High heat resistance, chemically inert vibration dampener	Brittle, low-impact resistance
Epoxy-modified PF	Better heat resistance than PF	Base is still PF and highly toxic
Thermoplastic polyimide resin	Abrasion resistance; does not exhibit thermal fade**	Thermal conductivity three times lower than PF

*Condensed polynuclear aromatic resin

**Thermal degradation

Fillers are frequently incorporated in the brake pad materials in order to reduce manufacturing costs and improve some properties and manufacturability [29].

The common fillers used in the friction materials are listed in Table 2. In particular, rubber particle fillers can be added to suppress brake noise and improve toughness and impact strength of friction materials [27]. Incorporating rubber components into polymer-based materials is a conventional method to improve flexibility and damping properties of the resulting polymer products [30].

Table 2 Common Fillers Used in Friction Materials [6].

Fillers	Descriptions
Barium sulfate	Imparts heat stability to friction material, aids friction characteristic
Calcium carbonate	Imparts heat stability to friction material
Mica	Suppresses low-frequency brake noise but causes interlayer splitting in friction material
Vermiculite	Suppresses low-frequency brake noise but has low heat resistance
Alkali metal titanates	Promotes stability of the friction coefficient
Molybdenum trioxide	Prevents thermal fade and cracking of friction lining under high-temperature conditions
Cashew dust	Suppresses brake noise but does not adhere well to friction material
Rubber dust	Suppresses brake noise but does not adhere well to friction material

Reinforcing fibers play a major role in maintaining stiffness, strength, and tribological behavior of friction composites [31]. Different kinds of reinforcing fibers, such as aramid pulp [32], carbon fiber [33], glass fiber [34], and natural fiber [35], have been employed in substitution to asbestos in brake pad composites to improve mechanical and thermal properties. Some properties of reinforcing fibers used in friction materials were listed in the Table 3.

Table 3 Reinforcing Fiber Types Used in Friction Materials [6].

Components	Advantages	Disadvantages
Glass	Sufficiently thermally resilient (high melting temperature of 1430 °C) but will start to soften at 600 °C	Brittle
Metallic	Thermally resilient steel and copper have melting temperature greater than 1000 °C	Large amounts may cause excessive rotor wear; may corrode
Aramid	Good stiffness to weight ratio; excellent thermal resilience; and good wear resistance	Soft; cannot be used without other fibers
Potassium titanate (a type of ceramic)	Thermally resilient (high melting temperature of 1371 °C) very hard; good wear resistance	Health hazard
Sepiolite	Thermally resilient (high melting temperature of 1550 °C); able to absorb traces of fluid	Potential health hazard
Ceramic	Thermally resilient (high melting temperature of 1700–2040 °C); good stiffness weight ratio	Brittle

Friction additives are components added to friction materials in order to modify the friction coefficients as well as the wear rates [36], as listed in Table 4. They are divided into two main categories: lubricants and abrasives. Lubricants assist in stabilizing frictional properties, particularly at high braking temperatures. Abrasives serve to increase friction, maintain cleanliness between contact surfaces, and limit the build-up of transfer films. Common examples include graphite and various metal sulfides such as antimony trisulfide (Sb_2S_3), aluminum oxide, iron oxides, silicon oxide, and zirconium silicate [36, 37].

Table 4 Types of Friction Additives for Friction Materials [6].

Friction Additives	Descriptions
Graphite	Widely used lubricant, available in natural or synthetic forms and as flakes or powder; able to form a self-sustaining lubricant layer
Metal sulfides	Good lubricating properties and lower thermal conductivities than graphite; included antimony/tin/copper/lead/sulfides
Metal oxides/silicates	Abrasives with hardness ranging from 500 HV (quartz) to 1750 HV (aluminum oxide); examples include quartz (SiO ₂), zirconium silicate, zirconium oxide, aluminum oxide, etc.

2.2 Benzoxazine Resin

Benzoxazine is a molecule where an oxazine ring (a heterocyclic six-membered ring with oxygen and nitrogen atom) is attached to a benzene ring [8]. There are several benzoxazine structures depending on the position of the heteroatoms as shown in the Figure 4.

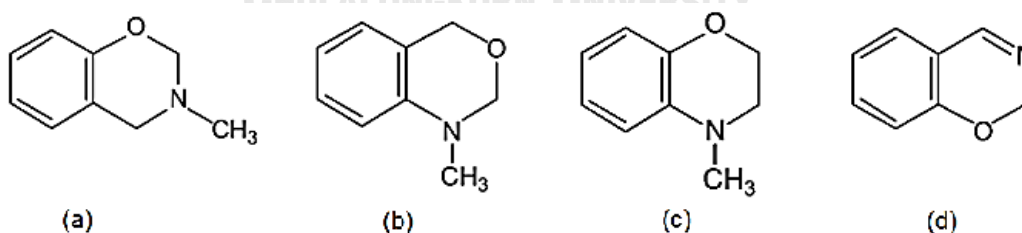


Figure 4 Various Types of Benzoxazine Monomer: (a) 3-Methyl-2H, 4H-Benzo[e]1,3-oxazine, (b) 1-Methyl-2H,4H-Benzo[d]1,3-oxazine, (c) 4-Methyl-2H,3H-Benzo[e]1,4-oxazine, and (d) 2H-Benzo[e]1,3-oxazine [8].

Holly and Cope [38] first reported the synthesis of benzoxazine in 1944. And, in the 1950s to 1960s, Burke [39, 40] significantly contributed to the fundamental understanding of the small molecular weight benzoxazine chemistry. Benzoxazine resins could be generally classified into monofunctional, bifunctional as well as multifunctional types depending on a type of phenol used [39]. These resins can be readily synthesized by a combination of a phenolic derivative, formaldehyde, and a primary amine as shown in Figure 5. A popular benzoxazine monomer synthesized from bisphenol-A (abbreviated as “BA”) and aniline (abbreviated as “a”) has an abbreviated monomeric benzoxazine name of BA-a [8]. Naming of polybenzoxazine is very complex due to the rich variety of structures from similar raw materials available [41]. When it is polymerized, one could simply describe this as “PBA-a” [8, 26].

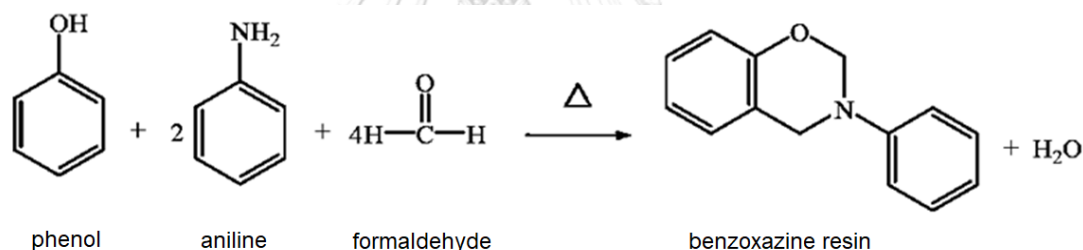


Figure 5 Synthesis of an Aniline Based Benzoxazine Resin (BA-a) [8].

Any combination of a bifunctional phenol and primary amine could be used. In a similar manner, any combination of a bifunctional amine and mono-functional phenol could also be used though the structure of the cross-linked polymer was somewhat different [8]. An example of the synthesis of a conventional type of benzoxazine resin, that was, bisphenol A / aniline-based (BA-a), was shown in Figure 6 [26]. After ring-opening polymerization of benzoxazine monomers, polybenzoxazine overcomes many shortcomings of traditional phenolics, such as using an acid or base catalyst and releasing condensation by-products; meanwhile it can have good

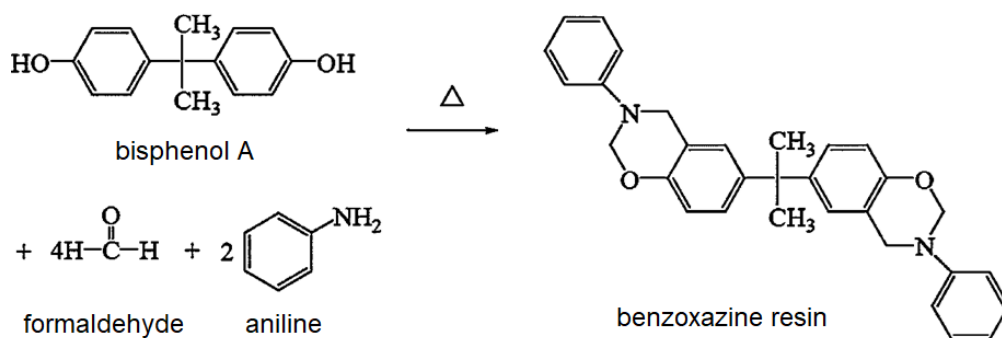


Figure 6 Synthesis of a Bifunctional Benzoxazine Monomer [26].

thermal properties and flame retardance of phenolics [28]. It should be cautioned that benzoxazine polymerization is not thermal polymerization as this term implies the thermal cleavage of a bond followed by free radical polymerization by the newly formed free radicals [8, 26].

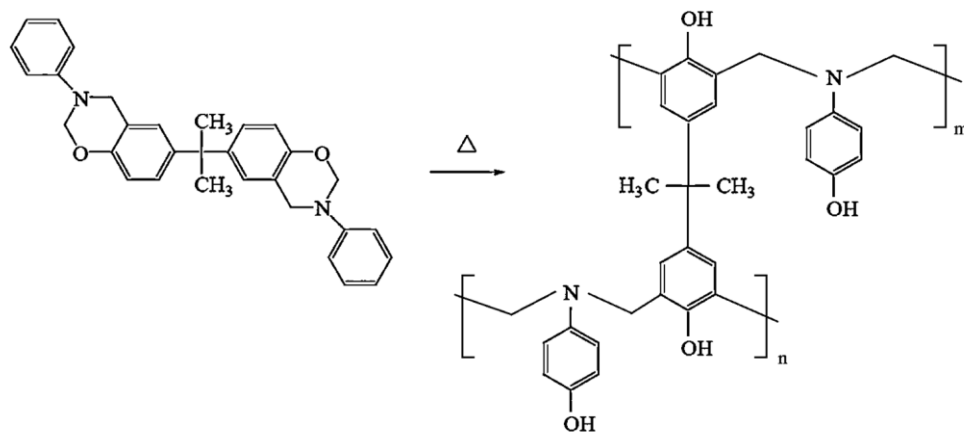


Figure 7 Polymerization of Benzoxazines [8].

Benzoxazines polymerize via a thermally induced ring-opening reaction to form a phenolic structure, as shown in Figure 7 [42]. Thus, it should be more appropriately called thermally accelerated (or activated) polymerization if the effect of temperature needed to be mentioned [26]. The ring opening polymerization is readily achieved by heating the purified monomer, typically at temperatures in the

range between 160 and 220 °C, and gelation takes place in a matter of minutes to tens of minutes at these temperatures if no initiators or catalysts are added [14, 28].

The properties of polybenzoxazines depend on their molecular structures; alterations in the chemical structures of benzoxazines can thus change the thermal stability of the corresponding polybenzoxazines. Polybenzoxazine has been reported to provide excellent thermal, mechanical, electrical, chemical, and physical properties such as high moduli, high glass-transition temperature, high char yield, near-zero volumetric shrinkage upon polymerization, low water absorption, low melt viscosity, excellent resistance to chemicals and UV light, and no by-product during cure [43, 44]. Furthermore, polybenzoxazines offer high thermal stability which is possibly due to the effects of the Mannich bridges by the intramolecular hydrogen bonding between the phenolic hydroxyl groups and the nitrogen atom of the Mannich bridge [4, 45]. According to Ishida and Sanders [42], thermal properties of polybenzoxazines can be improved by varying amine groups.

In this study, benzoxazine resins synthesized via a noncatalytic synthesis method from bisphenol-A, formaldehyde, and five different types of arylamines i.e., o-toluidine, p-toluidine, aniline, m-toluidine, 3,5-xylidine, as shown in Figure 8, were used as potential binders for brake pads. Table 5 showed the thermal properties of the resulting arylamine-based benzoxazine resins [26].

Table 5 Thermal Properties of Arylamine-Based Polybenzoxazines [26].

Properties	BA-ot	BA-pt	BA-a	BA-mt	BA-35x
Glass Temperature, T _g (°C)	114	209	168	209	243
Char yield (% at 800 °C)	32	31	30	31	28
Temperature at 1% wt. loss (°C)	220	264	276	300	305
Temperature at 5% wt. loss (°C)	228	305	315	350	350

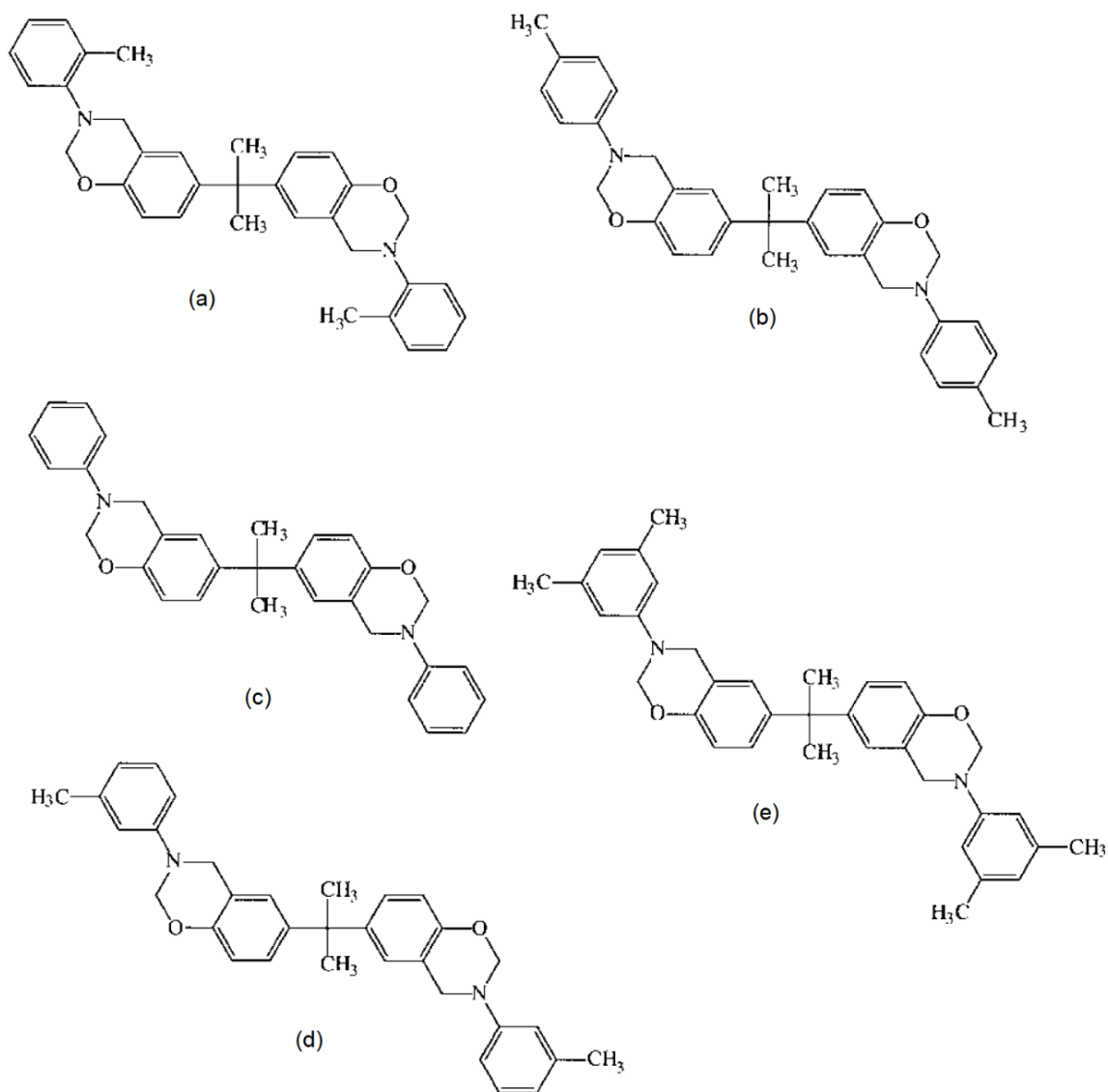


Figure 8 Benzoxazine Resins from Different Alkyl-Substituted Aromatic Amines:

- (a) 6,69-Bis(3-(2-Methyl) Phenyl-3,4-Dihydro-2H-1,3-Benzoxazinyl) Isopropane (BA-ot),
 (b) 6,69-Bis(3-(4-Methyl) Phenyl-3,4-Dihydro-2H-1,3-Benzoxazinyl) Isopropane (BA-pt),
 (c) 6,69-Bis(3-Phenyl-3,4-Dihydro-2H-1,3-Benzoxazinyl) Isopropane (BA-a),
 (d) 6,69-Bis(3-(3-Methyl)-Phenyl-3,4-Dihydro-2H-1,3-Benzoxazinyl) Isopropane (BA-mt),
 (e) 6,69-Bis(3-(3,5-Dimethyl)Phenyl-3,4-Dihydro-2H-1,3-Benzoxazinyl) Isopropane (BA-35x) [42].

2.3 Kinetics of Polymer Degradation

Kinetics of polymer degradation are typically expressed using parameterized degressive rate that links the three main variables of polymer degradation [46]. These were the conversion of the reaction (α), pressure (P), and temperature (T). The rate is denoted as per the following equation,

$$\frac{d\alpha}{dt} = k(T) f(\alpha) \quad (1)$$

where α is conversion of the reaction, t is time (min), $f(\alpha)$ is the reaction model (conversion dependent process) that represents the degradation mechanism following a reaction order, n , and $k(T)$ is function given by the Arrhenius equation [47]. The pressure variable is typically ignored in the majority of kinetic studies, regardless of the fact that it has a noted effect on the kinetics of degradation [46]. Each variable in the above equation is given a symbol and linked with a mathematical function, where α is typically expressed as per the following:

$$\alpha = \frac{m_0 - m}{m_0 - m_f} \quad (2)$$

where m is the weight of the sample (g) at time t ; m_0 is the initial weight (g) of the sample; and m_f is the final weight (g) of the completely decomposed sample [46]. It is assumed that k follows the Arrhenius equation [47],

$$k(T) = A \exp\left(\frac{-E_a}{RT}\right) \quad (3)$$

where A stands for the pre-exponential (or frequency) factor (min^{-1}), E_a is the apparent activation energy (J/mol), and R is the universal gas constant ($\text{J K}^{-1} \text{mol}^{-1}$).

Substituting 'k(T)' to the rate equation to obtain,

$$\frac{d\alpha}{dt} = A \exp\left(\frac{-E_a}{RT}\right) f(\alpha) \quad (4)$$

According to non-isothermal kinetic theory, thermal degradation at a constant heating rate, $\beta = dT/dt$, with a unit of (K min⁻¹), could be expressed by

$$\frac{d\alpha}{dT} = \frac{A}{\beta} \exp\left(\frac{-E_a}{RT}\right) f(\alpha) \quad (5)$$

Generally, the activation energies can be calculated by using three well-known methods for dynamic heating experiment, i.e., Kissinger method, Flynn-Wall-Ozawa method, and Coats-Redfern method [46].

2.3.1 Isoconversional methods

All isoconversional methods take their origin in the isoconversional principle that states that the reaction rate at constant extent of conversion is only a function of temperature. This can be demonstrated by taking the derivative of the reaction rate to obtain [48]

$$\left[\frac{\partial \ln(d\alpha/dt)}{\partial T^{-1}}\right]_{\alpha} = \left[\frac{\partial \ln k(T)}{\partial T^{-1}}\right]_{\alpha} + \left[\frac{\partial \ln f(\alpha)}{\partial T^{-1}}\right]_{\alpha} \quad (6)$$

where the subscript α indicates isoconversional values, i.e., the values related to a given extent of conversion. Because at $\alpha = \text{const}$, $f(\alpha)$ is also constant, and the second term in the right hand side of Eq. (6) is zero. Thus,

$$\left[\frac{\partial \ln(d\alpha/dt)}{\partial T^{-1}}\right]_{\alpha} = -\frac{E_a}{R} \quad (7)$$

It follows from Eq. (7) that the temperature dependence of the isoconversional rate can be used to evaluate isoconversional values of the activation energy, E_a , without assuming or determining any particular form of the reaction model. For this reason, isoconversional methods are the model-free methods [49]. Two of the most extensively used isoconversional method are those proposed by Kissinger (Differential Method) and Ozawa (Integration Method) that provide accurate values of activation energies even if they were a function of the reacted fraction [47, 48].

2.3.2 Kissinger Method (Differential Method) [51].

The Kissinger method is an overwhelmingly popular way of estimating the activation energy of thermally stimulated processes [50]. The advantage of this method is that the activation energy could be obtained without the knowledge of any thermal degradation reaction mechanism in advance. If the general rate equation is differentiated by parts, and at the maximum of the reaction exothermic peak, $T = T_p$, then rate equation becomes:

$$0 = \frac{df(\alpha)}{dT} + f(\alpha) \frac{E_a \beta}{RT^2} \quad (8)$$

Solving for β/T_p^2 and taking the natural logarithm, yields:

$$\ln\left(\frac{\beta}{T_p^2}\right) = \ln\left(\frac{AR}{\beta E_a}\right) + \ln[n(1-\alpha_p)^{n-1}] - \frac{E_a}{RT_p} \quad (9)$$

Kissinger method uses Eq. (9) to determine the activation energy of solid-state reactions, where T_p and α_p are the absolute temperature and weight loss at maximum weight-loss rate $(d\alpha/dt)_p$, respectively, and n is the reaction order. The Kissinger method is based upon a series of experiments in which small milligram quantities of the reacting material are heated at several heating rates while the

reaction exothermic peaks are recorded [51]. From the slope of the straight-line $\ln(\beta/T_p^2)$ versus $1/T_p$, the activation energy, E_a , can be obtained.

2.3.3 Flynn-Wall-Ozawa Method (Integration Method) [52].

This method could be employed to quantify the activation energy without knowing of the reaction mechanisms. Flynn-Wall-Ozawa method is presented in Equation (10),

$$\log \beta = \log\left(\frac{AE_a}{g(\alpha)R}\right) - 2.315 - \frac{0.457E_a}{RT} \quad (10)$$

where T (K) is the absolute temperature, α is conversion, β (K min^{-1}) is the heating rate, E_a is the activation energy, R is the gas constant, A (min^{-1}) is pre-exponential factor, and $g(\alpha)$ is the function that represented an integral form of the thermal decomposition. By this method, the activation energies of the thermal degradation process of the brake pad composites were determined from the slope of the straight-line $\log \beta$ versus $1/T$ at constant value of conversion [52].

2.3.4 Coats-Redfern Method [52].

Besides the above two methods, Kissinger and Flynn-Wall-Ozawa method, the Coats-Redfern method [53, 54] is often used in kinetic analysis of solid-state processes. The Coats-Redfern method is presented in Equation (11),

$$\ln \frac{g(\alpha)}{T^2} = \ln\left(\frac{AR}{\beta E_a}\right) - \frac{E_a}{RT} \quad (11)$$

The activation energy can be directly obtained from the slope of the straight line resulting from the plot of the left-hand side of the equation as a function of $1/T$, and

A is obtained from the intercept of the plot, where α is conversion and T (K) is the absolute temperature. A is the frequency factor, E_a is the activation energy, R is the universal gas constant, and β ($K \text{ min}^{-1}$) is the heating rate. The $g(\alpha)$ represents function commonly used for description the thermal decomposition [55, 56].

2.3.5 Criado Method

Criado et al. [57, 58] had proposed a method which can accurately determine the reaction mechanism in the solid-state reaction process, which $Z(\alpha)$ function is defined as

$$Z(\alpha) = \frac{(d\alpha/dt)}{\beta} \pi(x) T \quad (12)$$

where x is defined as E_a/RT and $\pi(x)$ is an approximate expression obtained by integration against temperature, reasonably proposed by Paterson [59],

$$\pi(x) = x e^x P(x) \quad (13)$$

And the relation $P(x)$ was proposed by Senum and Yang [52],

$$P(x) = \left(\frac{e^{-x}}{x} \right) \left(\frac{x^3 + 18x^2 + 86x + 96}{x^4 + 20x^3 + 120x^2 + 240x + 120} \right) \quad (14)$$

when $x > 20$, the error of Equation (14) is less than $10^{-5}\%$. Combining the above equation yields the master curve as shown in Equation (15),

$$Z(\alpha) = f(\alpha) g(\alpha) \quad (15)$$

This equation was used to plot the $Z(\alpha)$ - α curves for different models listed in Table 6 [60], whereas the relation,

$$Z(\alpha) = \frac{d\alpha}{dT} \frac{E_a}{R} e^{E_a/RT} P(x) \quad (16)$$

could be derived from Equation (12) with $\beta = dT/dt$ and substituted x for E_a/RT . The Equation (16) was used for representing the experimental curve. By comparing the experimental and master curves (Equation (15)), the mechanism type of the thermal degradation could be identified.



Table 6 Algebraic Expressions for $g(\alpha)$ and $f(\alpha)$ for the Most Frequently Used Mechanisms of Solid-State Processes [52].

Mechanism	$g(\alpha)$	$f(\alpha)$
A2, Nucleation and growth (Avrami equation (1))	$[-\ln(1 - \alpha)]^{1/2}$	$2(1 - \alpha)[- \ln(1 - \alpha)]^{1/2}$
A3, Nucleation and growth (Avrami equation (2))	$[-\ln(1 - \alpha)]^{1/3}$	$3(1 - \alpha)[- \ln(1 - \alpha)]^{2/3}$
A4, Nucleation and growth (Avrami equation (3))	$[-\ln(1 - \alpha)]^{1/4}$	$4(1 - \alpha)[- \ln(1 - \alpha)]^{3/4}$
R1, Phase boundary-controlled reaction (one-dimensional movement)	α	1
R2, Phase boundary-controlled reaction (contracting area)	$[1 - (1 - \alpha)^{1/2}]$	$2(1 - \alpha)^{1/2}$
R3, Phase boundary-controlled reaction (contracting volume)	$[1 - (1 - \alpha)^{1/3}]$	$3(1 - \alpha)^{2/3}$
D1, One-dimensional diffusion	α^2	$1/(2\alpha)$
D2, Two-dimensional diffusion (Valensi equation)	$(1 - \alpha)\ln(1 - \alpha) + \alpha$	$[- \ln(1 - \alpha)]^{-1}$
D3, Three-dimensional diffusion (Jander equation)	$[1 - (1 - \alpha)^{1/3}]^2$	$(3/2)[1 - (1 - \alpha)^{1/3}]^{-1}(1 - \alpha)^{2/3}$
D4, Three-dimensional diffusion (Ginstling Brounshtein equation)	$[1 - (2/3)\alpha] - (1 - \alpha)^{2/3}$	$(3/2)[1 - (1 - \alpha)^{1/3}]^{-1}$
F1, Random nucleation with one nucleus on the individual particle	$-\ln(1 - \alpha)$	$1 - \alpha$
F2, Random nucleation with two nuclei on the individual particle	$1/(1 - \alpha)$	$(1 - \alpha)^2$
F3, Random nucleation with three nuclei on the individual particle	$1/(1 - \alpha)^2$	$(1/2)(1 - \alpha)^3$

2.4 Deconvolution Method

The method that involves the deconvolution of the individual processes from the overall differential kinetic curves obtained under linear heating rate conditions, followed by the kinetic analysis of the discrete processes was proposed and recommended [61]. The computer program, Seasolve Peakfit®, was used for nonlinear least-squares curve fitting and the functions that were not included as standard functions were introduced as user-defined functions. In this context, based on curves of thermograms, the deconvolution technique was carried out to split the overlapped degradation peaks into several distinct peaks in sequence, corresponding to material components in the friction composite. Some mathematical functions would be selected for deconvoluting an overlapped peak. The selection of the functions is heuristic, and the choice of a function is based on the shape analysis of the single-step reactions. Different conventional mathematical fitting functions have been tested for deconvolution, paying special attention to the shape analysis of the kinetic curves. It has been shown that many conventional mathematical curves such as the Gaussian, Weibull, Fraser-Suzuki, and Lorentzian ones fit kinetic curves inaccurately and the subsequent kinetic analysis yields incorrect kinetic parameters [48, 61]. Bi-Gaussian is a piecewise function, i.e., it is an asymmetric function characterized by its shape factors and possesses the capabilities of reflecting the asymmetric shapes of a peak by setting the peak highest point as its center value [62]. Therefore, Bi-Gaussian function was employed to capture the real asymmetric shapes of thermal degradation of the friction composites, herein.

CHAPTER III

LITERATURE REVIEWS

Ning and Ishida [28] synthesized bi-functional benzoxazine. The benzoxazine (BA-a) was found to have good mechanical and thermal properties with good capacity for composite manufacturing, i.e., tensile modulus of 3.2 GPa, and tensile strength of 58 MPa. Furthermore, they reported that BA-a was more flexible than conventional phenolic resins. In terms of molecular design, no by-products were generated during polymerization step and no solvent was needed for the synthesis of resin. The results suggested that the bi-functional benzoxazine could be an interesting thermosetting resin for use as the binder matrix of friction composite material because of no release of by-product upon curing and they have good thermal and mechanical properties.

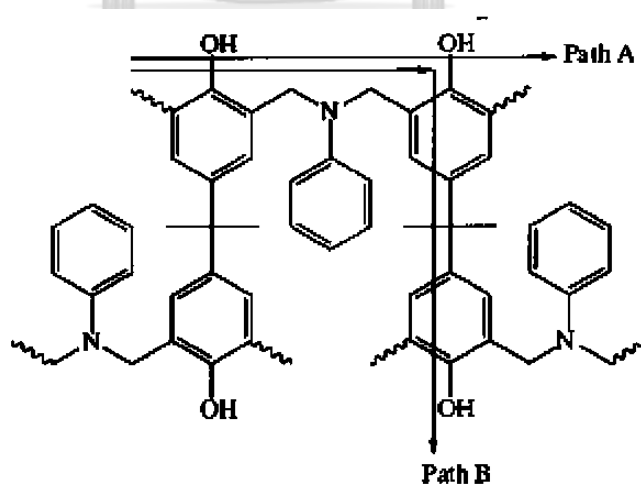
Kurihara et al. [63] reported the use of polybenzoxazine as binder in friction materials. They found that the wear rate of friction material based on polybenzoxazine was lower than the one based on phenolic resin (PF). Moreover, the friction material based on phenolic resin had cracks upon molding. The cracks were generated during the curing step, which generated ammonia gas as by-product. The results suggested that benzoxazine resin can be used as the binder of friction materials.

Wu et al. [64] studied the effect of glass transition temperature of thermosetting matrices on friction and wear properties of friction material. Phenolic resin, benzoxazine resin, benzoxazine-phenolic copolymer and benzoxazine-phenolic-nitrile butadiene rubber copolymer were used as binders. The modified benzoxazine resins were found to provide the higher mechanical and thermal properties, and the lower curing temperature as shown in Table 7.

Table 7 Thermal Properties of Binders [58].

Binder	Curing Temperature (°C)	Glass Transition Temperature (°C)
Phenolic resin	130	250
Benzoxazine resin	180	203
Benzoxazine-Phenolic copolymer	170	225
Benzoxazine-Phenolic-Nitrile Butadiene Rubber copolymer	135	230

The regioselectivity of some arylamine-based benzoxazine polymerization was proposed by Ishida and Sanders [65]. The network structure of the cured materials is expected. The structure of BA-a is similar to the phenolic Mannich bridge network as shown in Figure 9, and, in addition, for meta substituted compound, BA-mt and BA-35x contain additional amounts of arylamine Mannich bridges, as

**Figure 9** The Phenolic Mannich Bridge Network Formation [60].

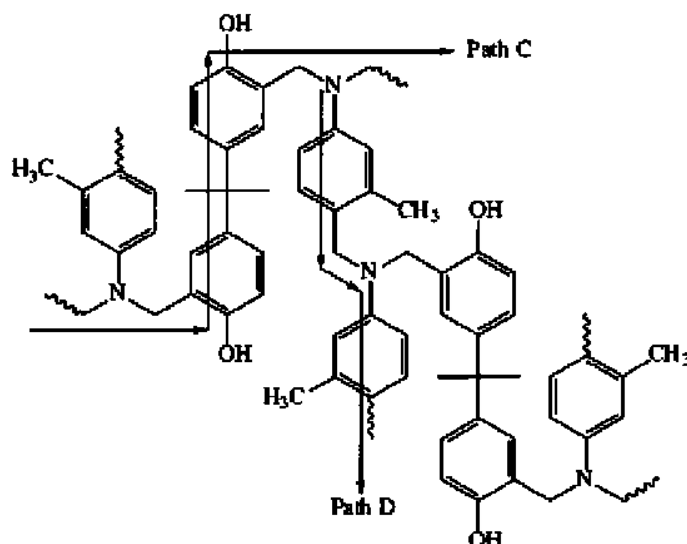


Figure 10 The Arylamine Mannich Bridge Network Formation [60].

can be seen in Figure 10 [45, 66]. As a consequence, the additional arylamine Mannich bridges significantly resulted in a higher glass transition temperature in BA-*mt* at 209 °C, and BA-35*x* at 243 °C, than BA-*a* at 168 °C. For materials based on *m*-toluidine and 3,5-xylydine, the onset of thermal degradation could be delayed until around 350 °C. Therefore, polybenzoxazine with additional amount of arylamine Mannich bridges and methylene bridges showed improvement in mechanical properties and higher crosslink densities [45]. Correlations between the observed mechanical properties and network structures were established. This study also confirmed that bi-functional benzoxazine monomers from Bisphenol A, Paraformaldehyde and Aromatic amine (aniline, *o*-toluidine, *m*-toluidine, *p*-toluidine and 3,5-xylydine) would improve crosslink density and showed high thermal stability and good mechanical property.

Low and Ishida [67] used two benzoxazine dimers, methyl-dimer and amyl-dimer, as the research subjects to study the thermal degradation mechanism by TGA-FTIR and GC-MS. TGA results showed that both dimers had a main degradation stage at around 200 °C. Two kinds of degradation process of the dimers in Figure 11 were proposed based on the cleavage of C–N and C–C, respectively. Because of lower covalent bond energy in the C–N bond (72 kcal/mol) than C–C bond (82.6 kcal/mol),

the weaker C–N may be easier to break following route (I) at a low temperature of 200 °C which leads to the major weight loss event. The more stable C–C bond will break at a higher temperature and follows route (II).

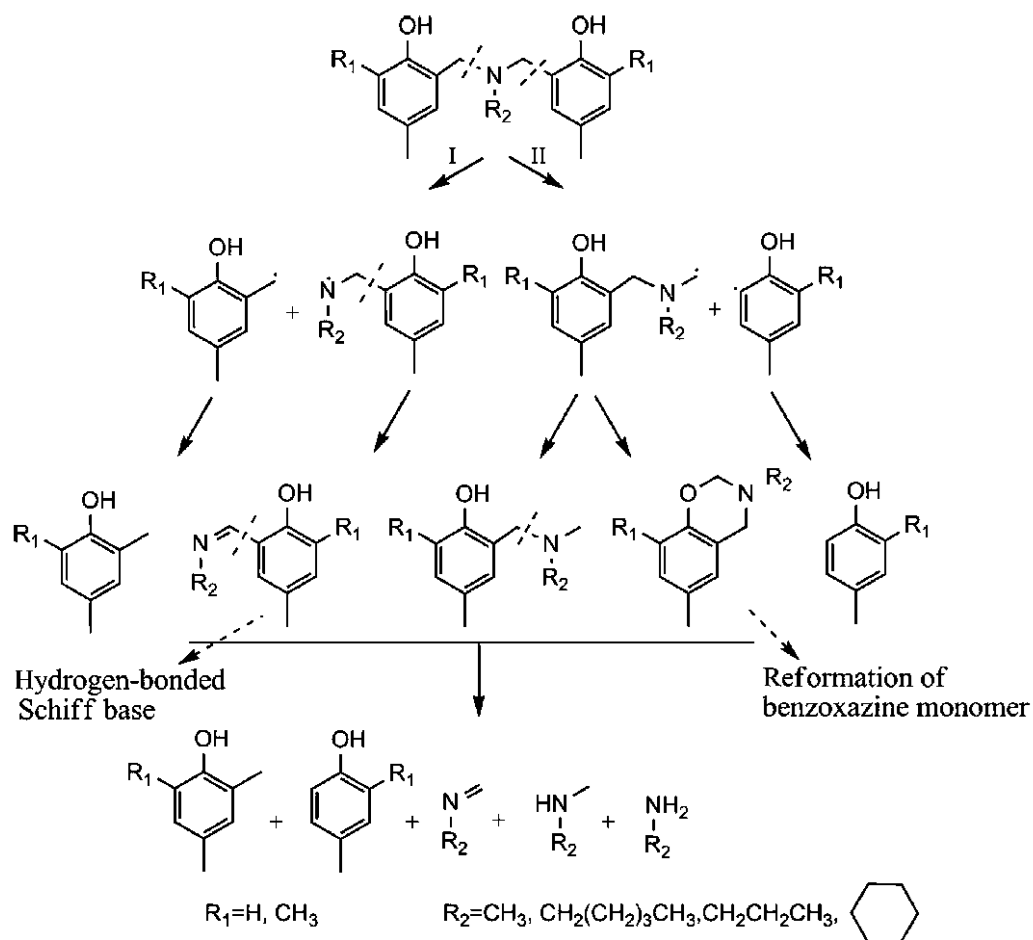


Figure 11 Proposed Degradation Process of Mannich Base Cleavage in Benzoxazine Dimer [63].

As seen in Figure 11, the Schiff base structure is formed from the cleavage of the C–N bond while the secondary amine is formed from the cleavage of the C–C bond. This is a main difference between two degradation routes. Valliyappan et al. [68] conducted TG/DTG-MS combined analysis on the new brake pad formulations.

Mass spectroscopy results indicated evolution of gases during the temperature ramp especially after 400 °C and were related to the physical-chemical reaction of the raw ingredients. The method of detecting changes in weight as a function of temperature under defined atmospheric condition is termed thermogravimetric analysis. Derivative thermogravimetric is the time rate of reaction derived from the TG results. In view of the possibility of materials discharging gases during the temperature ramp, TGA is usually approached in tandem with evolved gas analysis such as mass spectroscopy. Jubsilp et al. [69] studied a kinetic of thermal degradation of bisphenol-a-aniline type polybenzoxazine (PBA-a) modified with benzophenone tetracarboxylic dianhydride (BTDA). The activation energy values obtained by Flynn-Wall-Ozawa method of five stages were 151, 232, 228, 217 and 352 kJ/mol. Furthermore, the appropriate conversion model of the degradation processes was studied by Criado method of the five stages [70]. The degradation reaction mechanism of five stages of the PBA-a:BTDA copolymer system was accounted by random nucleation model with one nucleus on the individual particle (F1).

CHAPTER IV

EXPERIMENTAL

4.1 Raw Materials

Benzoxazine resin was synthesized based on the traditional method [8]. The bisphenol A, paraformaldehyde, and aniline (AR grade) were obtained from PTT Phenol (Bangkok, Thailand), the Merck Company (Darmstadt, Germany), and Panreac Quimica SA Company (Barcelona, Spain), respectively, and o-toluidine, p-toluidine, m-toluidine, and 3,5-xylidine (AR grade), were purchased from Loba Chemie Ltd. (Bangkok, Thailand). Carbon and glass fibers were purchased from S J Sinthuphun Trading (Bangkok, Thailand) and Toho and Beslon Carbon (Tokyo, Japan), respectively. Aramid pulp was provided by DuPont (Tokyo, Japan). Iron fibers, friction modifiers, and fillers were provided by Compact International (Bangkok, Thailand).

4.2 Preparation of Benzoxazine Resin

Polybenzoxazine resins were generally prepared by thermally activated polymerization of benzoxazines as shown in Figure 12. According to the reported method [8, 45], aniline-based benzoxazine monomers were synthesized from bisphenol-A, para-formaldehyde, and aniline at the ratio of 1:4:2. The mixture was heated at approximately 110 °C in an aluminum pan and was mixed rigorously for about 30-45 min to yield the light-yellow solid resin product. The same method was used to synthesize o-toluidine-based benzoxazine resin (BA-ot), p-toluidine-based benzoxazine resin (BA-pt), m-toluidine-based benzoxazine resin (BA-mt), and 3,5-xylidine-based benzoxazine resin (BA-35x).

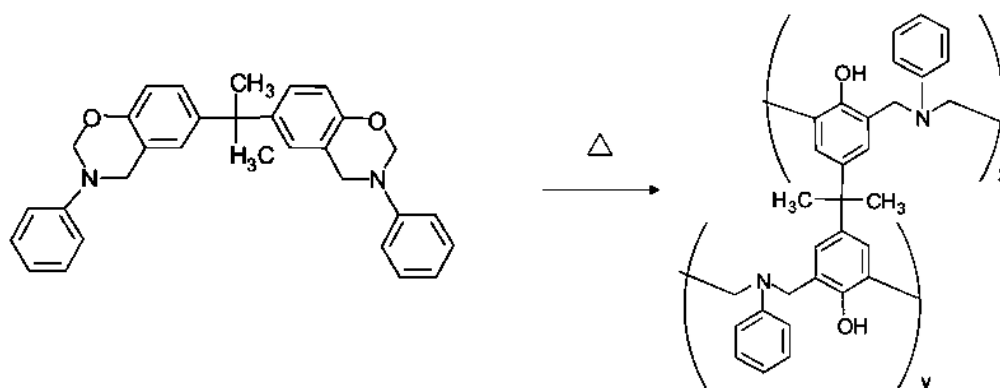


Figure 12 Polymerization of Benzoxazines Monomer BA-a [8].

4.3 Synthesis of Compositd Friction Material

Each type of five benzoxazine monomers was used to prepare friction material composites with the composite formulation following Akebono's patent no. US5360842A [63] with some modifications as summarized in Table 8. Each molding formulation was mixed at 120 °C for 40–45 min using an internal mixer to ensure uniform mixing. The compound was placed in iron mold with specified dimensions and then heated in a compression molder at 200 °C at a pressure of 15 MPa (using a hydraulic press) for 2 h. The fully cured composites were cooled to room temperature before being tested and characterized.

Table 8 Formulation of Polybenzoxazine Composite Friction Material

Ingredients	Binder	Reinforcing Fibers			
	PB resin	Aramid pulp	Carbon fiber	Glass fiber	Iron fiber
Content (wt%)	10	3.75	1.25	10	25

Ingredients	Friction modifiers		Fillers		
	Graphite	ZrSiO ₄	BaSO ₄	Rubber dust	Cashew dust
Content (wt%)	7	25	10	4	4

4.4 Sample Characterization

Thermogravimetric analysis was carried out and recorded on a thermogravimeter (model TGA1 STARe System from Mettler-Toledo) as shown in Figure 13. Degradation temperature at 5% weight loss (T_{d5}) and char yield of all polybenzoxazines and arylamine based benzoxazine friction composites were studied. The TGA experiments were carried out from room temperature (25 °C) to the temperature about 1000 °C under nitrogen atmosphere with various heating rates of 1, 5, 10, 20 and 25 °C/min, respectively. The purge nitrogen gas flow rate was maintained at 80 ml/min. The sample mass used was measured to be approximately 10-15 mg. Char yield of the above specimens were reported at 800 °C. The corresponding derivative thermogravimetric (DTG) curves of the composites were analyzed by Seasolve Peakfit© program to determine the thermal degradation steps



Figure 13 Thermal Gravimetric Analyzer (TGA): Model TGA1 STARe from Mettler-Toledo

and their activation energies. The kinetic parameters of thermal degradation were determined by Kissinger method, Flynn-Wall-Ozawa method, and Coats-Redfern method, which were based on the principle that the reaction rate at constant extent of conversion were only a function of temperature (iso-conversional method). Additionally, thermal degradation mechanisms were also determined by Criado method.



CHAPTER V
RESULTS AND DISCUSSION

5.1 Effects of Types of Arylamines Based Benzoxazine Binder on Thermal Stability of Brake Pad Composites

Thermal degradation and thermal stability are two of crucial key thermal parameters for evaluating practical performances of composited friction materials. Thermogravimetric analysis (TGA) is a technique where a change in a sample mass is monitored as a function of temperature (T) or time (t). In this study, degradation

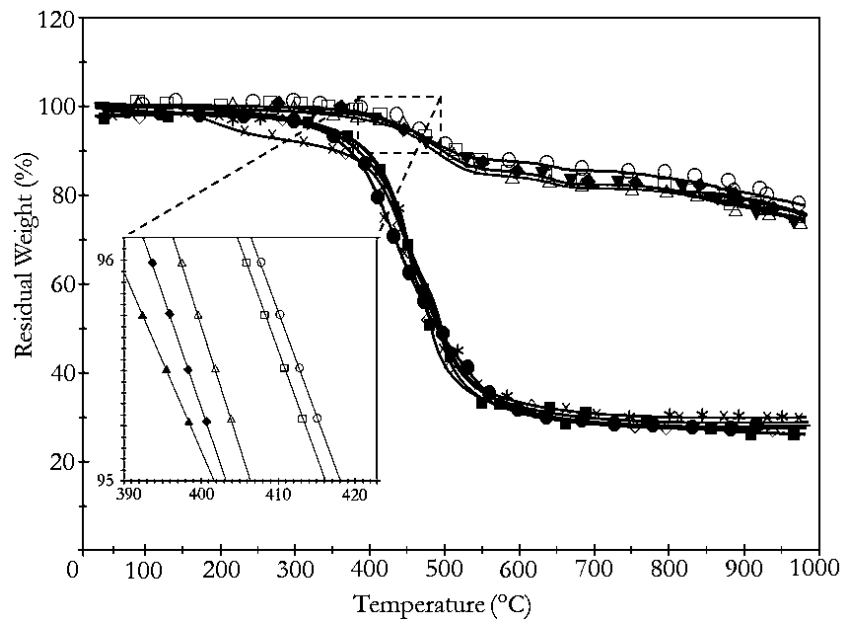


Figure 14 TGA Thermogram from Degradation of Polybenzoxazine and Friction Composites Prepared from Different Benzoxazine Resin: (x) BA-ot Polybenzoxazine, (*) BA-pt Polybenzoxazine, (●) PBA-a Polybenzoxazine, (◇) BA-mt Polybenzoxazine, (■) BA-35x Polybenzoxazine, (▲) BA-ot based Friction Composite, (◆) BA-pt based Friction Composite, (Δ) BA-a based Friction Composite, (□) BA-mt based Friction Composite, (O) BA-35x based Friction Composite

temperatures of the polymer composites were defined as the temperature at 5% weight loss and the char yields were obtained at 800 °C under nitrogen atmosphere for each composite. Five different arylamines based benzoxazines (BA-ot, BA-pt, BA-a, BA-mt and BA-35x) composites were selected to represent different types of brake pads in this study. Figure 14 showed the relationship between residual weight (%) and temperature (°C) from polybenzoxazines and arylamines based benzoxazine composites. The char yield determined at 800 °C and weight loss data for each composite were also collected and presented in Table 9. The inset of Figure 14 explained the relationship between the thermal decomposition temperatures at 5% weight loss and the types of arylamines based benzoxazine in the composite. It clearly showed that the decomposition temperatures of the composites were increased from about 225, 302, 310, 348, and 352 °C to about 402, 403, 406, 414 and 418 °C for BA-ot, BA-pt, BA-a, BA-mt and BA-35x based binder friction composite, respectively. The char yields of the composites were also increased from about 32, 32, 30, 31, and 30% to about 78, 79, 80, 82, and 83% for BA-ot, BA-pt, BA-a, BA-mt and BA-35x based binder friction composite, respectively. These decomposition

Table 9 Weight Loss Data and Char Yield from Thermal Decomposition in Nitrogen Atmosphere

Samples	5% weight loss (°C)	Char yield (wt%)
Polybenzoxazine BA-ot	225.4 ± 0.2	31.7 ± 0.2
Polybenzoxazine BA-pt	302.3 ± 0.2	32.3 ± 0.2
Polybenzoxazine BA-a	310.7 ± 0.2	30.2 ± 0.1
Polybenzoxazine BA-mt	348.6 ± 0.5	30.9 ± 0.2
Polybenzoxazine BA-35x	352.2 ± 0.3	29.7 ± 0.1

Table 9 (cont.) Weight Loss Data and Char Yield from Thermal Decomposition in Nitrogen Atmosphere

Samples	5% weight loss (°C)	Char yield (wt%)
BA-ot based composite	402.3 ± 0.3	78.2 ± 0.5
BA-pt based composite	403.3 ± 0.6	78.7 ± 0.3
BA-a based composite	406.2 ± 0.1	80.3 ± 0.2
BA-mt based composite	414.4 ± 0.2	81.6 ± 0.1
BA-35x based composite	418.3 ± 0.2	83.4 ± 0.2

temperature at 5% weight loss and char yields of arylamine-based friction composites were in the same range as that reported by Jubsilp et al. [71] who reported the thermal stability and degradation temperature of ultrafine acrylonitrile butadiene rubber (UFNBRPs)-modified arylamine based polybenzoxazine friction composite to be at 410 °C and 80% char yield. In addition, comparatively, the T_{d5} and residual weight values of brake pads in this research from different benzoxazine types were higher than those of phenolic composites (commercial brake pads) which were at 390 °C and 63%, respectively [72]. The higher thermal stability of polybenzoxazine composite material was related to higher degree of crosslink density of benzoxazine network bridge (Mannich bridge) leading to the hindrance of polymer network mobility which were tightly bound with fibers and other ingredients [33, 42]. The amount of crosslink density of binder in benzoxazine composites could be indicated by the storage modulus in the rubbery state of benzoxazine composites [42]. The approximation expressed in the Equation (14) below, as proposed by Nielsen [73], showed the relationship between storage modulus at rubbery state and

crosslink density. From Table 10, the storage modulus in rubbery state [72], increasing in the order of BA-ot, BA-pt, BA-a, BA-mt and BA-35x, were 1.12, 1.45, 1.63, 1.87 and 2.39 GPa, respectively.

$$\log \frac{E_e}{3} = 7.0 + 294 \rho_x \quad (17)$$

Where E_e = equilibrium tensile storage modulus in rubbery plateau (dyne/cm²)

ρ_x = crosslink density which described the mole number of network chains per unit volume (mol/cm³)

Crosslink densities of friction materials, calculated from Equation (14), were increased in the order of BA-ot, BA-pt, BA-a, BA-mt and BA-35x, as shown in Table 10. BA-ot based friction composite was the least thermally stable compound, with the crosslink density about 8.76 mmol/cm³. Ran et al. [74] mentioned that the reason for this phenomenon was due to an anchoring of the pendent rings through reaction at the para position which significantly decrease the backbone crosslink density and the thermal stability. From Table 10, the crosslink density of BA-35x friction composite was higher than other materials suggesting that this resin based composite material appeared to be able to better resist polymer segmental motion with filler reinforced because the methyl group that located on the meta site of arylamine ring helped increase the amount of phenolic Mannich bridges, arylamine Mannich bridges and methylene bridges resulting in higher crosslink densities [65]. In BA-35x and BA-mt, the composited network structure was not a pure phenolic Mannich bridge network but contained additional structures, like those found in an arylamine Mannich bridge network and various methylene bridges [42].

Table 10 Storage Modulus and Crosslink Density of Polybenzoxazine Composite Friction Materials

Benzoxazine composite	Storage modulus at rubbery state (GPa)	Crosslink density (mmol/cm ³)
BA-ot	1.12	8.76
BA-pt	1.45	9.12
BA-a	1.63	9.27
BA-mt	1.87	9.51
BA-35x	2.39	9.88

In addition, according to Sander [65], for BA-35x based friction composite, the main chain does not involve any Mannich bridge structures that are ortho to a phenolic moiety. These bridges that are ortho to a phenolic moiety simply are acting as crosslinks. Therefore, the arylamine Mannich bridge structures that comprise the main chain which was not ortho to a phenolic moiety could degrade at a higher temperature and, hence, delay the onset of weight loss. However, the more rigid network created by the methylene linkages created kinetic barriers to weight loss as well [42]. From this result, the BA-35x based friction composite was selected for further kinetic studies of composite system since it provided the maximum decomposition temperature and char yield.

5.2 Analysis of Thermal Degradation Kinetic of Friction Composite

After obtaining the TGA and DTG curves, Seasolve Peakfit© program was used to separate the DTG curve of the composite of the BA-35x based binder. As seen in Figure 15, at heating rate of 20 °C/min, the BA-35x based friction composite began to lose weight at ca. 260 °C and reached the maximum rate at ca. 450 °C. After resolving the DTG curve by using the computer software, Seasolve Peakfit©, by setting thermogravimetric data stream with deconvoluted method, as a result, it was noticed that the DTG curve of the composite, presented in Figure 15, composes of a three-stage weight-loss process.

In addition, from Figure 15, the derivative thermograms for thermal degradation of friction composite at heating rate of 20 °C/min showed six peaks of weight-loss process, centered approximately at 397, 454, 526, 584, 722, and 827 °C for peak 1, peak 2, peak 3, peak 4, peak 5, and peak 6, respectively.

Peak 1 and 2, which occurred at ca. 397 and 454 °C, respectively, concerned the degradation of neat polybenzoxazine in the composite binder. This result was in good agreement with the study of Hemvichian et al. [75], who reported that this degradation process occurred with 2 peaks observed at 400 and 460 °C, respectively. Peak 1 which occurred at ca. 400 °C represented the degradation of phenolic linkage in polybenzoxazine where the phenolic compound means the group of aromatics with hydroxyl group [8]. Peak 2 represented the decomposition of the Schiff base of the polybenzoxazine where the Schiff base is a basic compound with the general structure $R_1R_2C=NR'$ from the condensation reaction between amine and aldehyde or ketone [8, 70]. Peak 3 occurred at ca. 500-530 °C which corresponded to the degradation of cashew dust [73]. Peak 4 and 5 were observed for the degradation of nitrile-butadiene rubber (NBR) and aramid pulp, which occurred at ca. 580 and 720 °C, respectively, as shown in Figure C1-b, c [73, 76] in the Appendix. Finally, Peak 6 displayed the degradation of barium sulphate as per Figure C1-d in the Appendix which approximately occurred at 800-850 °C [76].

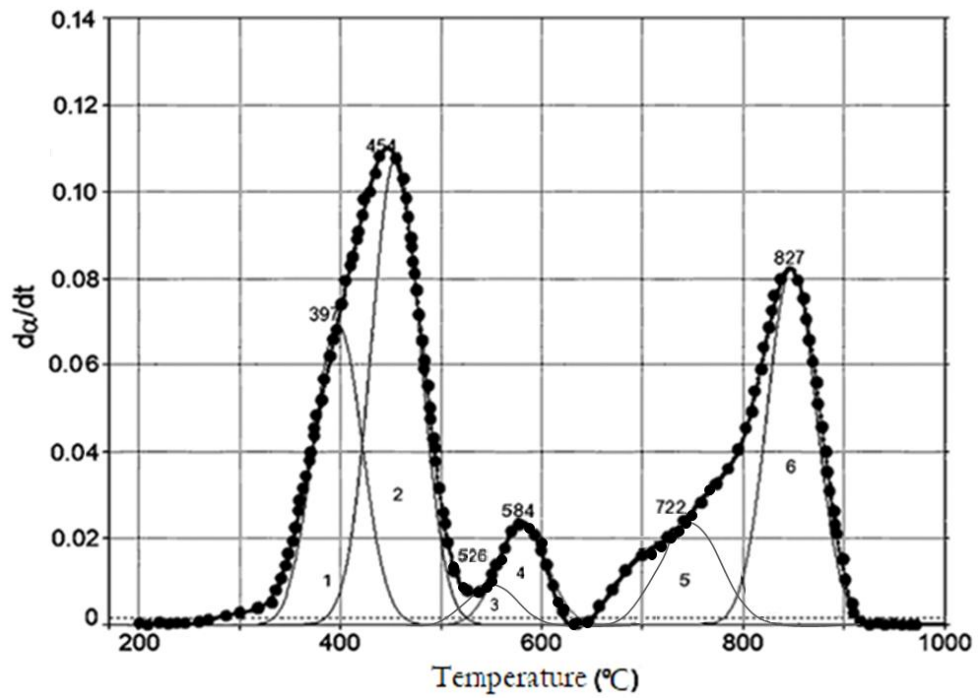


Figure 15 Derivative TGA Thermogram of BA-35x Brake Pad Composite and Its Separated Peaks by Using Simulation Software: (●) Experimental Data, (—) Simulated Curve (heating rate 20 °C/min)

5.3 Determination of Thermal Degradation Kinetic Parameters

The kinetic analysis and the activation energies (E_a) for the thermal degradation reaction of the BA-35x based friction composite material were estimated from Kissinger, Flynn-Wall-Ozawa and Coats-Redfern methods.

5.3.1 Kissinger Method (Differential Method)

The useful form of the Kissinger equation for estimating the activation energy, E_a , was shown in the Equation (9),

$$\ln\left(\frac{\beta}{T_p^2}\right) = \ln\left(\frac{AR}{\beta E_a}\right) + \ln[n(1-\alpha_p)^{n-1}] - \frac{E_a}{RT_p} \quad (9)$$

where	T_p	= absolute peak temperature (K)
	α_p	= weight loss at maximum weight-loss rate
	E_a	= activation energy (J/mol)
	β	= heating rate (K min ⁻¹)
	n	= reaction order
	A	= pre-exponential factor (min ⁻¹)
	R	= gas constant (J/mol)

From the Equation (9), the activation energy can be evaluated from the slope of the Kissinger plot of the straight-line $\ln(\beta/T_p^2)$ versus $1/T_p$ for various heating rates, 1, 5, 10, 20, and 25 °C/min. For peak 1, peak 2, peak 3, peak 4, peak 5, and peak 6, the activation energies were evaluated, from the straight-line slope of $-E_a/R$, to be 248.2, 281.3, 232.4, 115.5, 365.1 and 522.5 kJ/mol, respectively, as summarized in Table 11.

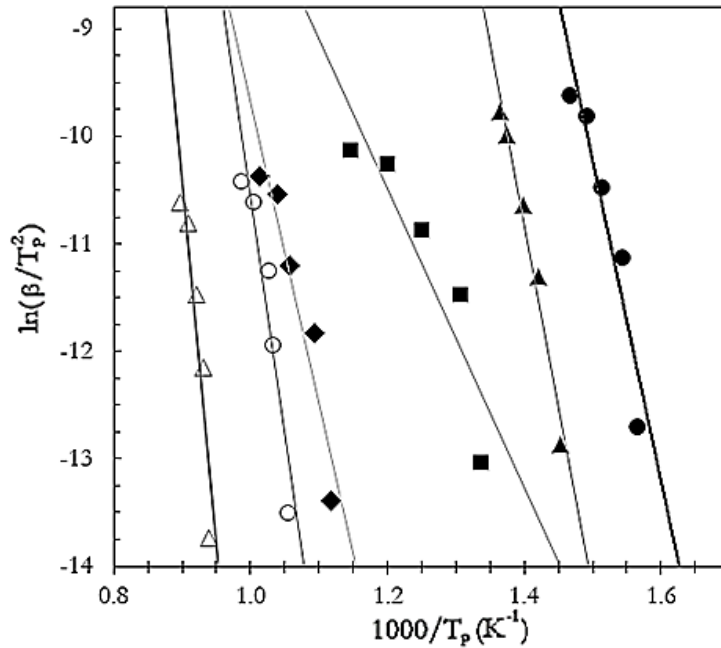


Figure 16 The Relation between $\ln(\beta/T_p^2)$ and $1000/T_p$ as per Kissinger Method (●) Peak 1, (▲) Peak 2, (◆) Peak 3, (■) Peak 4, (○) Peak 5, (△) Peak 6

Table 11 Activation Energies Determined by Kissinger Method for BA-35x Based Friction Composite from Different Heating Rates

Peak 1		Peak 2		Peak 3	
E_a (kJ/mol)	R^{2*}	E_a (kJ/mol)	R^{2*}	E_a (kJ/mol)	R^{2*}
248.2	0.9507	281.3	0.9679	232.4	0.9723

Peak 4		Peak 5		Peak 6	
E_a (kJ/mol)	R^{2*}	E_a (kJ/mol)	R^{2*}	E_a (kJ/mol)	R^{2*}
115.5	0.9469	365.1	0.9723	522.5	0.9276

*Correlation coefficient

5.3.2 Flynn-Wall-Ozawa Method (Integration Method)

Flynn–Wall–Ozawa method was relatively a simple method to calculate the value of activation energy from curve of weight loss versus temperature. This method could be applied to determine activation energies (E_a) without any knowledge of the reaction mechanisms [52] using the following equation,

$$\log \beta = \log \left(\frac{AE_a}{g(\alpha)R} \right) - 2.315 - \frac{0.457E_a}{RT} \quad (10)$$

where	T	= absolute temperature (K)
	α	= degree of transformation of the sample (conversion)
	$g(\alpha)$	= functions used for description of thermal degradation
	E_a	= activation energy (J/mol)
	β	= heating rate (K min ⁻¹)
	A	= pre-exponential factor (min ⁻¹)
	R	= gas constant (J/mol)

By this method, the activation energies, E_a , of the thermal degradation process of the brake pad composite were determined from the slope of the straight-line $\log \beta$ versus $1/T$ at constant value of fractional conversion as shown in Figure 17. The activation energies for the thermal degradation reactions followed peak 1, peak 2, peak 3, peak 4, peak 5, and peak 6, can be evaluated to be 241.4, 287.7, 219.1, 106.8, 363.1 and 531.4 kJ/mol, respectively.

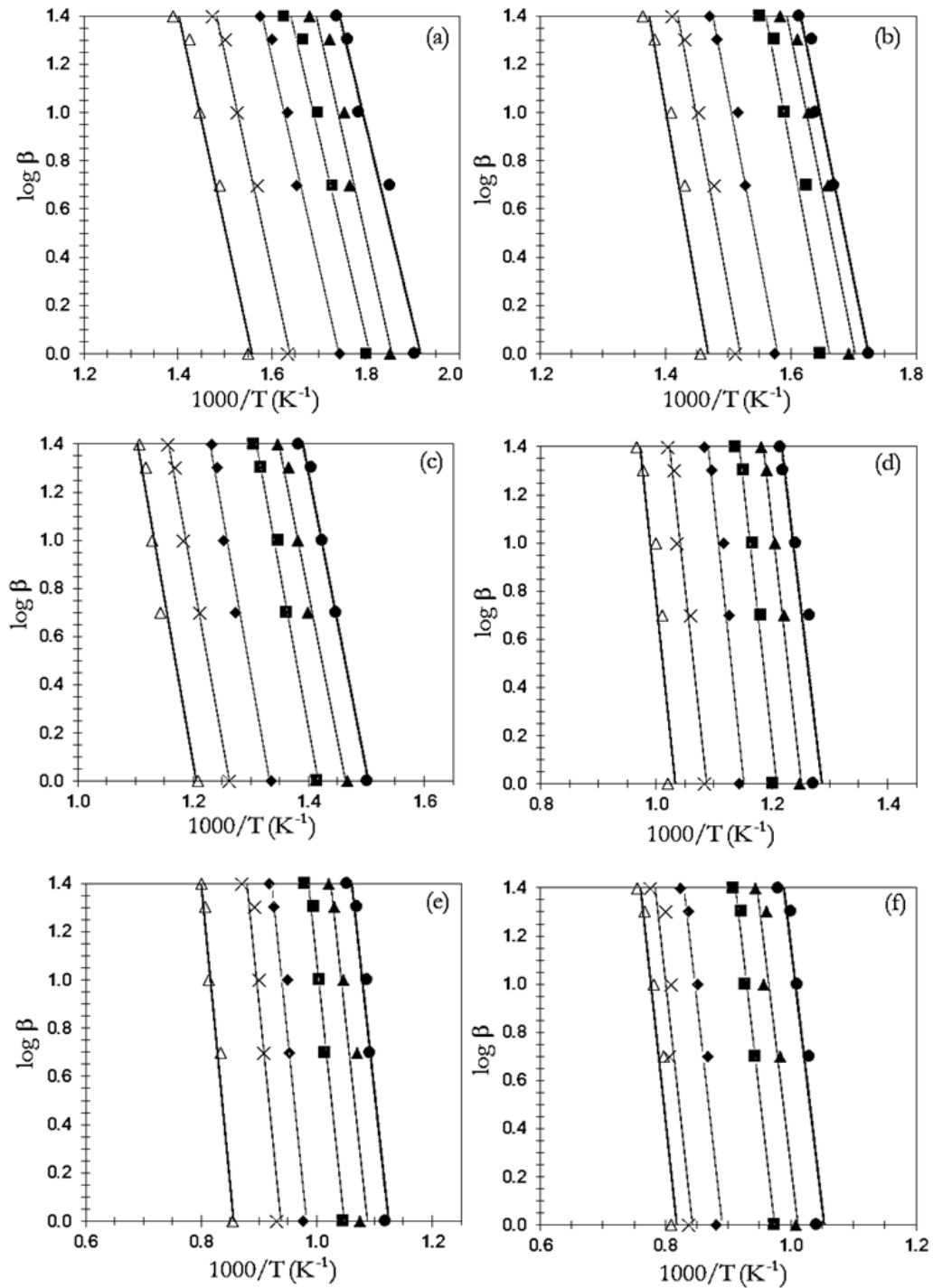


Figure 17 The Relation between $\log \beta$ versus $1000/T$ according to Flynn-Wall-Ozawa Method for BA-35x friction Composite for (a) Peak 1, (b) Peak 2, (c) Peak 3, (d) Peak 4, (e) Peak 5, and (f) Peak 6, with Conversion of (●) 10%, (▲) 20%, (■) 40%, (◆) 60%, (X) 80%, and (Δ) 100%.

Table 12 Activation Energies Obtained by Using Flynn-Wall-Ozawa Method for BA-35x Based Friction Composite at Various Conversions

conversion (%)	E_a (kJ/mol)	R^{2*}	E_a (kJ/mol)	R^{2*}	E_a (kJ/mol)	R^{2*}
	Peak1		Peak2		Peak3	
10	225.3	0.9769	267.3	0.9569	208.9	0.9563
20	234.8	0.9423	278.5	0.9556	212.3	0.9444
40	237.1	0.9126	285.6	0.9235	215.6	0.9542
60	244.2	0.9788	291.2	0.9485	218.6	0.9632
80	250.1	0.9291	298.8	0.9632	224.5	0.9874
100	257.4	0.9856	304.9	0.9514	235.2	0.9231
average	241.4		287.7		219.1	

conversion (%)	E_a (kJ/mol)	R^{2*}	E_a (kJ/mol)	R^{2*}	E_a (kJ/mol)	R^{2*}
	Peak4		Peak5		Peak6	
10	95.2	0.9236	319.8	0.9123	497.3	0.9587
20	99.2	0.9563	336.5	0.9361	512.1	0.9658
40	104.1	0.9514	345.9	0.9856	525.6	0.9123
60	108.3	0.9854	371.2	0.9203	541.3	0.9021
80	113.9	0.9658	382.6	0.9014	548.3	0.9632
100	119.8	0.9745	423.1	0.9874	564.3	0.9741
average	106.8		363.1		531.4	

*Correlation coefficient between experimental and theoretical master plot

5.3.3 Coats-Redfern Method

In order to determine kinetic parameters and thermal degradation mechanism, the Coats–Redfern method, which was given in Equation (11), was used:

$$\ln \frac{g(\alpha)}{T^2} = \ln \left(\frac{AR}{\beta E_a} \right) - \frac{E_a}{RT} \quad (11)$$

where	T	= absolute temperature (K)
	α	= degree of transformation of the sample (conversion)
	$g(\alpha)$	= functions used for description of thermal degradation
	E_a	= activation energy (J/mol)
	β	= heating rate (K min ⁻¹)
	A	= pre-exponential factor (min ⁻¹)
	R	= gas constant (J/mol)

According to this method, $g(\alpha)$ was the function that depended on reaction mechanisms and could be calculated from the relation described in Table 6. The activation energies (E_a) of the brake pad degradation process were determined from the slope of the straight-line $\ln [g(\alpha)/T^2]$ versus $1/T$ at different reaction mechanisms as shown in Figure 18. The model that gave the best linear fit was selected as the chosen model. Table 12 listed the calculated kinetic parameters for different models and compared with activation energies from the Kissinger and Flynn-Wall-Ozawa methods. These results showed that at the specified heating rate, the thermal degradation mechanism of composite could be explained by the Random nucleation with one nucleus on the individual particle (F1) because this mechanism presented the activation energies that were similar to the values obtained by iso-conversional methods above. As shown in Table 12, the activation energies for the thermal

degradation reaction F1 were approximately evaluated to be 244.5, 289.4, 221.8, 102.7, 344.7, and 525.2 kJ/mol for peak 1, peak 2, peak 3, peak 4, peak 5, and peak 6, respectively. This type of degradation mechanism was also confirmed by the Criado method in the next determination.



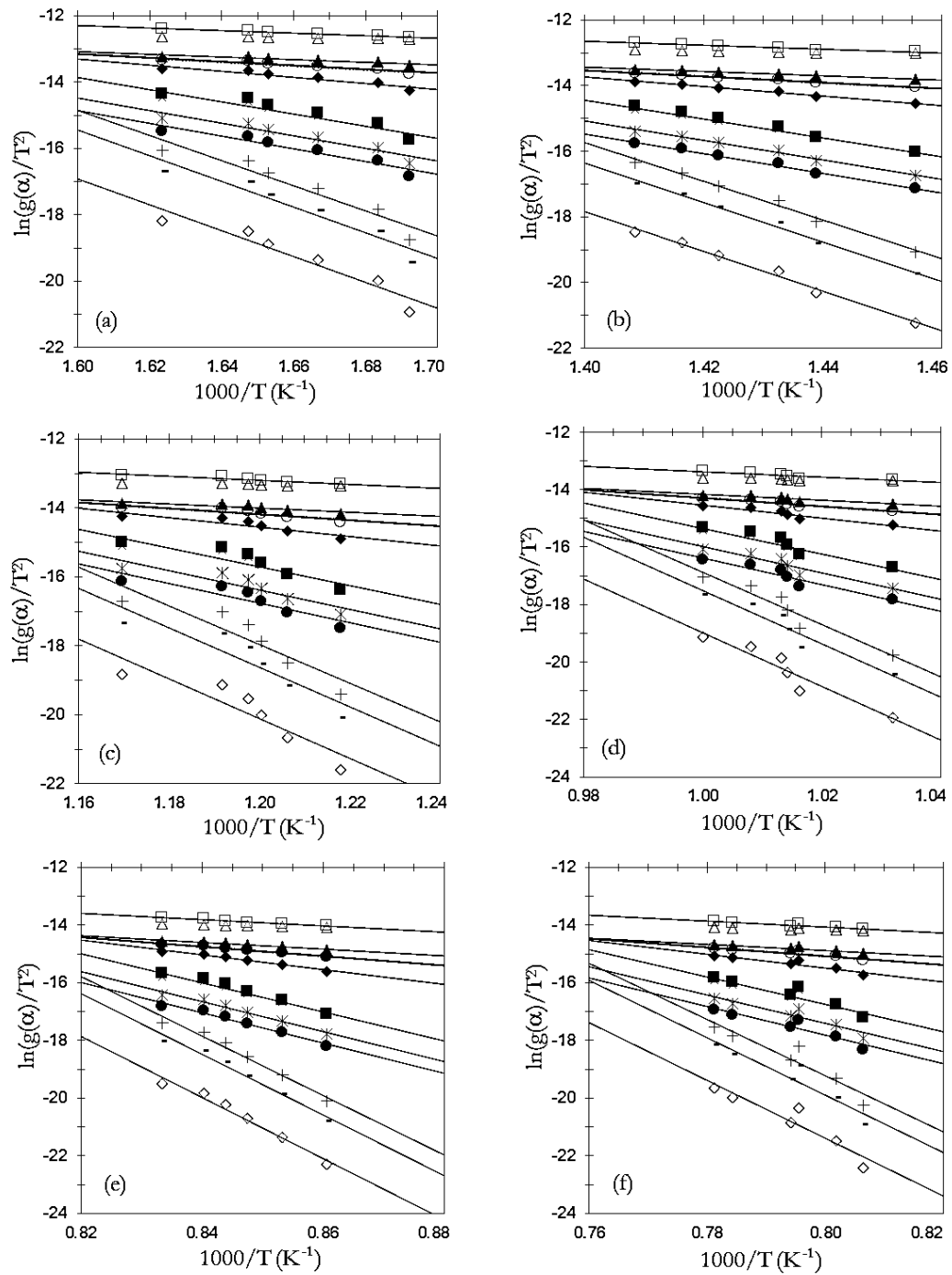


Figure 18 The Relation between $\ln(g(\alpha)/T^2)$ versus $1000/T$ according to Coat-Redfern Method for BA-35x Brake Pad Composites For Various Reaction Mechanism at The Heating Rate of $20\text{ }^\circ\text{C}/\text{min}$ for (a) Peak 1, (b) Peak 2, (c) Peak 3, (d) Peak 4, (e) Peak 5, (f) Peak 6, and Reaction Mechanism for (\blacklozenge) A2, (\circ) A3, (\blacktriangle) A4, (\times) R1, ($*$) R2, (\bullet) R3, ($+$) D1, ($-$) D2, ($-$) D3, (\diamond) D4, (\blacksquare) F1, (\triangle) F2, and (\square) F3.

Table 12 Activation Energies Obtained by Using Coats-Redfern Method for BA-35x Based Friction Composite for Various Conversions at 20 °C/min Heating Rate (Degradation Mechanisms: A2, A3, A4: Nucleation and Growth, R1, R2, R3: Phase Boundary-Controlled Reaction, D1, D2, D3, D4: 1, 2, 3-Dimensional Diffusion, F1, F2, F3: Random Nucleation)

Model	E _a (kJ/mol)	R ²	E _a (kJ/mol)	R ²	E _a (kJ/mol)	R ²
	Peak1		Peak2		Peak3	
A2	121.25	0.9547	113.72	0.9446	213.10	0.9864
A3	77.21	0.9523	71.17	0.9115	135.53	0.9956
A4	55.56	0.9611	49.89	0.9775	96.74	0.9806
R1	289.03	0.9463	226.07	0.9235	418.96	0.9415
R2	306.14	0.9841	233.63	0.9375	432.24	0.9632
R3	333.59	0.9713	236.20	0.9642	436.73	0.9514
D1	489.12	0.9035	466.07	0.9544	857.53	0.9464
D2	499.22	0.9415	476.04	0.9476	875.04	0.9846
D3	509.89	0.9232	486.33	0.9235	493.08	0.9702
D4	502.03	0.9586	479.47	0.9485	781.05	0.9235
F1	244.48	0.9215	289.38	0.9632	221.83	0.9484
F2	19.32	0.9865	17.43	0.9504	35.36	0.9233
F3	50.01	0.9122	48.79	0.9214	90.34	0.9895

Table 12 (cont.) Activation Energies Obtained by Using Coats-Redfern Method for BA-35x Based Friction Composite for Various Conversions at 20 °C/min Heating Rate (Degradation Mechanisms: A2, A3, A4: Nucleation and Growth, R1, R2, R3: Phase Boundary-Controlled Reaction, D1, D2, D3, D4: 1, 2, 3-Dimensional Diffusion, F1, F2, F3: Random Nucleation)

Model	E_a (kJ/mol)	R^2	E_a (kJ/mol)	R^2	E_a (kJ/mol)	R^2
	Peak4		Peak5		Peak6	
A2	188.19	0.9464	199.51	0.9964	124.17	0.9456
A3	120.01	0.9846	126.03	0.9876	75.82	0.9245
A4	85.92	0.9687	89.28	0.9732	51.65	0.9255
R1	369.70	0.9964	393.97	0.9687	252.96	0.9818
R2	381.08	0.9858	406.82	0.9864	261.00	0.9132
R3	384.93	0.9832	403.17	0.9956	263.72	0.9687
D1	755.75	0.9687	808.90	0.9235	926.79	0.9464
D2	770.75	0.9464	825.83	0.9485	837.39	0.9236
D3	586.21	0.9846	343.29	0.9532	448.31	0.9856
D4	775.90	0.9712	631.65	0.9514	641.03	0.9464
F1	102.72	0.9235	344.78	0.9564	525.22	0.9756
F2	30.75	0.9732	32.28	0.9856	12.37	0.9532
F3	77.84	0.9687	85.50	0.9752	45.61	0.9117

5.4 Thermal Degradation Mechanism of the Brake Pad Composites

According to the analysis by Coats-Redfern method, by evaluating and comparing the activation energies with the model, various possible mechanisms could be determined, for example, reaction mechanisms, R2, R3, and F1 were approximately evaluated from the thermal degradation with the corresponding activation energies obtained by the Kissinger and Flynn-Wall-Ozawa methods and so on for the other stages. The Criado model gave more information and was used as additional model to give the kinetics assessment of reactions and confirm the calculation result from Coats-Redfern method. The suggested kinetic models and the expressions, according to Table 6, of associated functions $f(\alpha)$ and $g(\alpha)$ could be used to construct the master curve, $Z(\alpha)-\alpha$, as shown in Equation (15) [58].

$$Z(\alpha) = f(\alpha) g(\alpha) \quad (15)$$

The plots for different mechanisms according to the Criado method for thermal degradation process of the brake pad composite were illustrated in Figure 19. The $Z(\alpha)-\alpha$, master curves could be plotted using Equation (15) according to different reaction mechanisms shown in Table 6. The experimental data obtained by iso-conversional method were substituted into Equation (16). Figure 19a-f showed the $Z(\alpha)-\alpha$, master and experimental curve of the BA-35x based friction composite. The results showed that the experimental curves of all six steps of degradation belonged to F1 reaction mechanism (random nucleation having one nucleus on individual particle). Comparable values of kinetic parameters and thermal degradation mechanism achieved by previous studies using various methods in literature were listed in Table E1 in the Appendix [14, 77-81]. It clearly showed that the activation energies of the friction composite in each peak increased from their pure

components. For example, theoretically the possible reason for synergism in the thermal stability was due to a large amount of arylamine Mannich bridges in the composite network with some additional chemical bonding between the benzoxazine binder and the other filler components. In addition, according to Table E1, some reactions of the pure component that occurred with molecular diffusional model (D1 reaction mechanism) could give rise to faster breakage of the macromolecules and to chemical structures that acted as stabilizer groups; however, in the composite this mechanism changed to the nucleation rate-controlled process (F1 reaction mechanism) during degradation. This degradation process followed the unimolecular nucleation mechanisms that the deterioration initiated from random points and acted as growth center for the development of the degradation reaction and, therefore, proceeded in the decomposition of random radicals where each bond of the same type had an equal probability for cleavage with a rate description according to a first order kinetic model [53, 82]. This type of mechanism contributed to the decrease in mobility of the reacting species from the enhancement of crosslink network of the friction composite, hence, the increase in more char yield and thermal degradation temperature of the composite [58, 67].

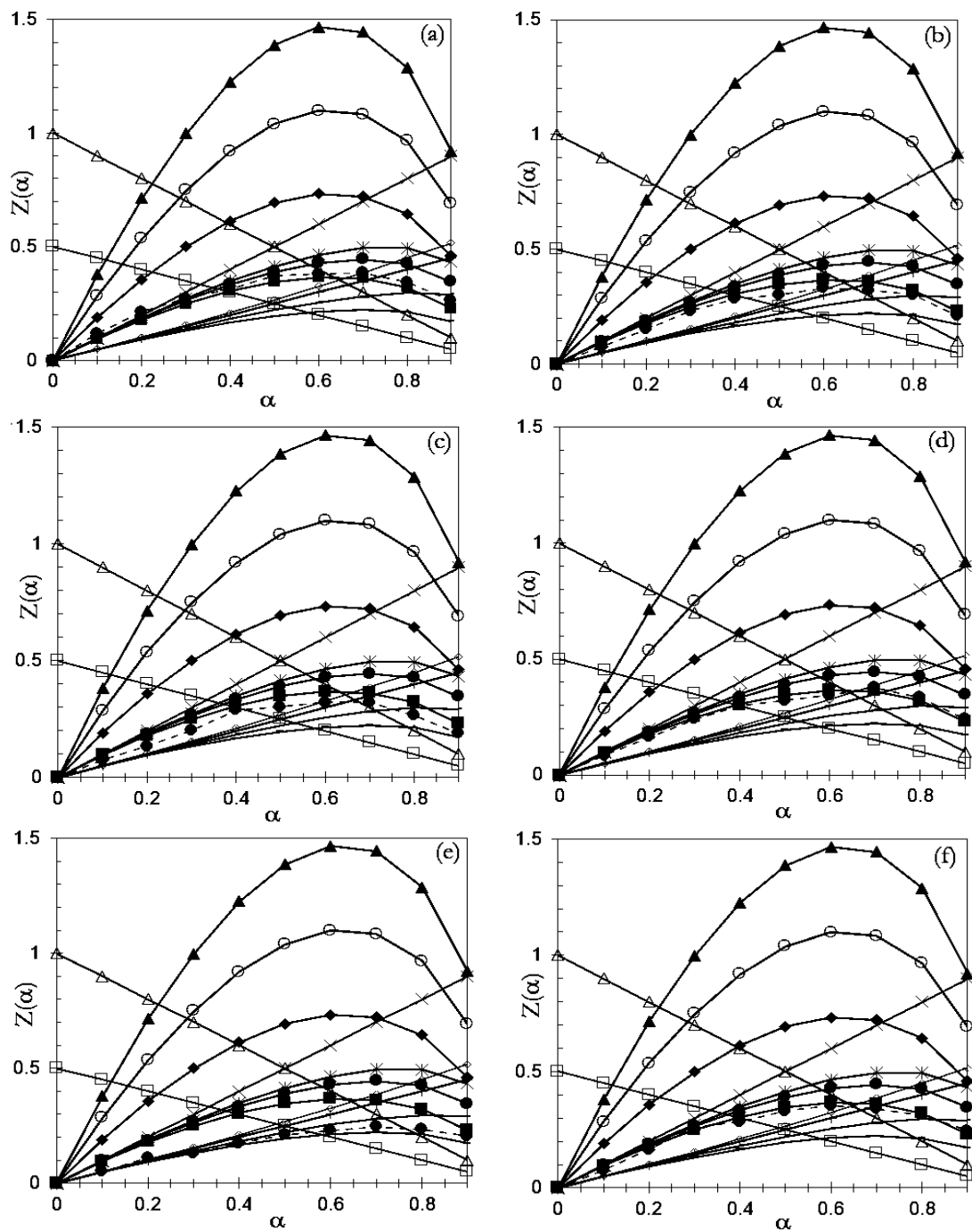


Figure 19 Theoretical Plots of $Z(\alpha)$ versus α (Master Curves) and Experimental Plot According to Criado Method of The BA-35x Based Friction Composite at Different Mechanisms for (a) Peak 1, (b) Peak 2, (c) Peak 3, (d) Peak 4, (e) Peak 5, (f) Peak 6, and Reaction Mechanism for (\blacklozenge) A2, (\circ) A3, (\blacktriangle) A4, (\times) R1, ($*$) R2, (\bullet) R3, ($+$) D1, ($-$) D2, (\leftarrow) D3, (\diamond) D4, (\blacksquare) F1, (\triangle) F2, (\square) F3 and (----) Experiment

CHAPTER VI

CONCLUSIONS

Friction composite materials from different polybenzoxazines based on different types of alkyl-substituted aromatic amines (BA-ot, BA-pt, BA-mt, BA-35x) exhibited high thermal stability with T_{d5} of 402-418 °C, and the BA-35x based composite was selected for further kinetic studies of composite system since it provided the maximum decomposition temperature and char yield. The investigation of thermal degradation processes and mechanisms of BA-35x based brake pad composite was carried out using thermogravimetric analysis technique under nitrogen atmosphere. The differentiation of thermogravimetric signal had detected six different peaks that showed degradation process of various components in the brake pad composite. The kinetic parameters, i.e., activation energies (E_a), were calculated by using Kissinger, Flynn-Wall-Ozawa, and Coats-Redfern methods. These three iso-conversional methods gave the corresponding values. From the Kissinger method, the activation energies for peaks 1 to 6 were evaluated to be 248, 281, 232, 115, 365 and 523 kJ/mol, respectively, whereas the activation energies obtained by Flynn-Wall-Ozawa method for peaks 1 to 6 were approximately estimated to be 241, 287, 219, 107, 363 and 531 kJ/mol, respectively, and by Coats-Redfern method, the activation energies were evaluated to be 244, 289, 222, 103, 344 and 525 kJ/mol for peaks 1 to 6, respectively. The activation energies from three methods were significantly consistent and the average values could be summarized to be 244, 286, 224, 108, 357 and 526 kJ/mol, respectively. Finally, the study of separated curves from Criado method indicated that the reaction mechanism of thermal degradation of BA-35x friction composite system followed the model of random nucleation with one nucleus on the individual particle (F1).

APPENDIX A

Arylamine-based Benzoxazine Resins Properties

Table A1 Thermal Properties of Arylamine-Based Polybenzoxazines

Monomer	Temperature 5% Weight Loss (°C)				Char Yield (wt%)			
	run1	run2	run3	avg.	run1	run2	run3	avg.
BA-ot	225.32	225.55	225.41	225.43	31.70	31.92	31.46	31.69
BA-pt	302.57	302.11	302.24	302.31	32.21	32.55	32.22	32.33
BA-a	310.71	310.54	310.95	310.73	30.21	30.25	30.14	30.20
BA-mt	348.28	348.48	349.11	348.62	30.94	30.79	31.14	30.96
BA-35x	352.29	351.74	352.56	352.20	29.74	29.82	29.69	29.75

APPENDIX B

Arylamine-based Benzoxazine Composite Properties

Table B1 Thermal Properties of Arylamine-Based Benzoxazines Friction Composite

Benzoxazine composite	Temperature 5% Weight Loss (°C)				Char Yield (wt%)			
	run1	run2	run3	avg.	run1	run2	run3	avg.
BA-ot	402.23	402.61	402.14	402.33	78.65	77.78	78.23	78.22
BA-pt	402.62	403.41	404.03	403.35	78.38	78.83	79.03	78.75
BA-a	406.25	406.13	406.16	406.18	80.49	80.75	80.53	80.59
BA-mt	414.57	414.35	414.22	414.38	81.55	81.67	81.62	81.61
BA-35x	418.53	418.22	418.08	418.28	83.58	83.21	83.42	83.40



Table B2 Initial Temperature, Peak Temperature, and Final Temperature (°C) of Peak 1 to Peak 6 for BA-35x based Friction Composite at Various Heating Rate

		Heating rate (°C/min)				
		1	5	10	20	25
Peak1	T _i	257.17	274.38	295.09	312.44	333.17
	T _p	365.13	374.26	386.89	397.25	408.01
	T _f	421.30	449.24	465.60	482.79	503.10
Peak2	T _i	351.45	365.97	384.60	402.23	422.46
	T _p	414.95	430.52	442.08	454.39	460.37
	T _f	459.67	476.49	495.54	514.05	534.80
Peak3	T _i	448.65	465.21	481.48	503.36	524.78
	T _p	448.35	475.23	492.32	526.45	549.32
	T _f	552.77	574.52	591.24	615.11	632.30
Peak4	T _i	558.07	579.79	593.31	621.33	642.68
	T _p	502.96	518.22	548.52	584.34	616.36
	T _f	698.85	713.06	738.19	759.82	779.40
Peak5	T _i	637.93	654.26	678.55	695.17	721.32
	T _p	659.12	674.35	698.21	722.83	745.20
	T _f	755.70	774.32	791.71	812.51	835.90
Peak6	T _i	705.61	729.08	743.11	765.54	781.59
	T _p	764.20	775.30	795.31	827.76	848.83
	T _f	845.19	867.58	884.38	906.36	925.61

Note: T_i = initial temperature, T_p = peak temperature, and T_f = final temperature

APPENDIX C

Thermal Properties of Some Friction Composite Ingredients

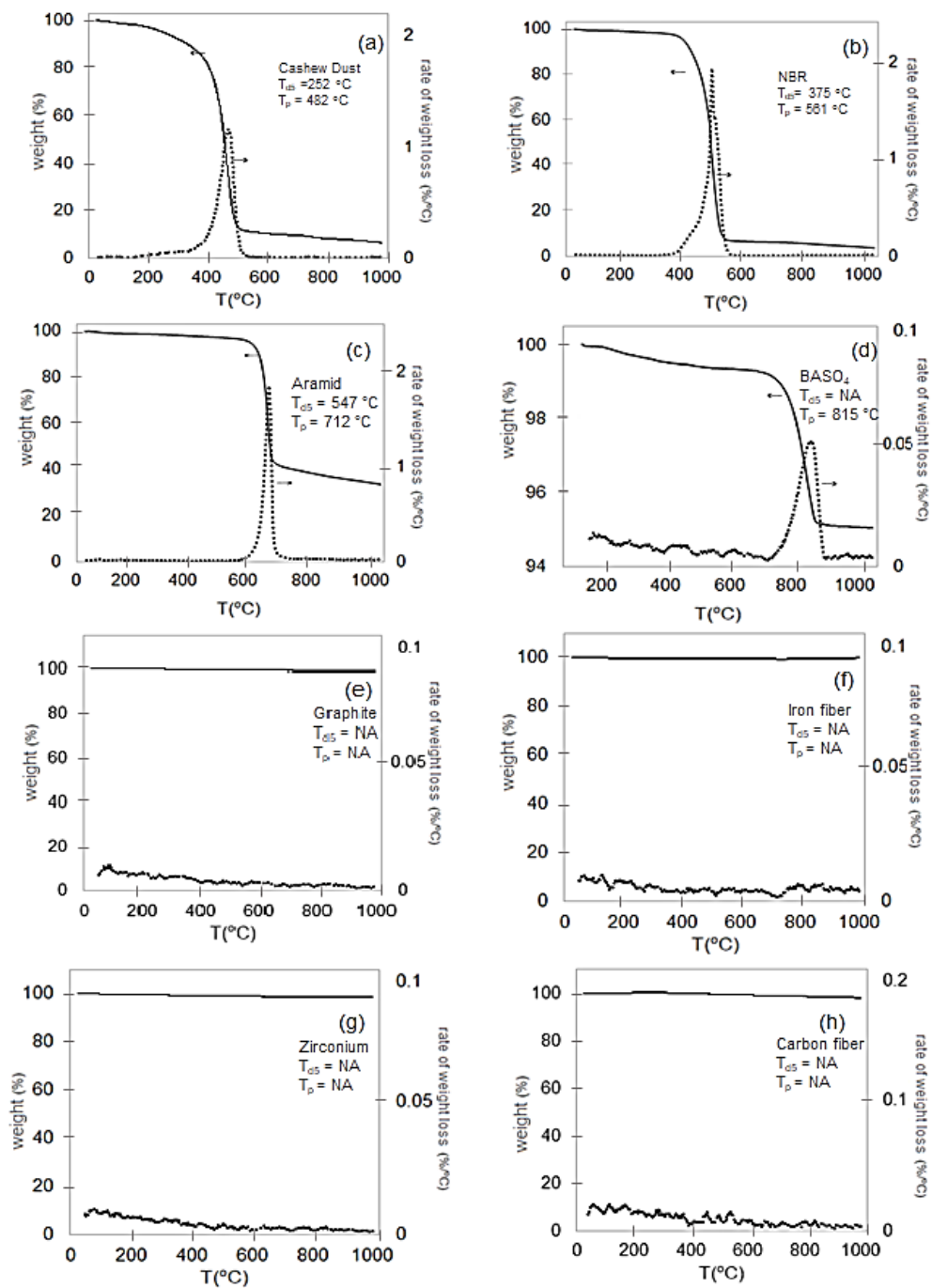


Figure C1 Thermogravimetry (TG) and the Corresponding Derivative Thermogravimetry (DTG) Curves of the Composite Ingredients for (a) Rubber dust (b) Cashew Dust (c) Aramid (d) BaSO_4 (e) Graphite (f) Iron Fiber (g) Zirconium (h) Carbon fiber

APPENDIX D

Thermal Data for Kinetics Analysis

Table D1 Relation between Heating Rate and Degradation Temperature Kissinger method of Peak 1 to Peak 6

	Heating rate (K/min)				
	1	5	10	20	25
Peak1					
T_p (K)	638.13	647.26	659.89	670.25	681.01
$1000/T_p$ (K ⁻¹)	1.567	1.545	1.515	1.492	1.468
$\ln(\beta/T_p^2)$	-12.917	-11.336	-10.682	-10.020	-9.828
Peak2					
T_p (K)	687.95	703.52	715.08	727.39	733.37
$1000/T_p$ (K ⁻¹)	1.454	1.421	1.398	1.375	1.364
$\ln(\beta/T_p^2)$	-13.067	-11.503	-10.842	-10.183	-9.976
Peak3					
T_p (K)	721.35	748.23	765.32	799.45	822.32
$1000/T_p$ (K ⁻¹)	1.386	1.336	1.307	1.251	1.216
$\ln(\beta/T_p^2)$	-13.235	-11.671	-11.065	-10.455	-10.323
Peak4					
T_p (K)	775.96	791.22	821.52	857.34	889.36
$1000/T_p$ (K ⁻¹)	1.289	1.264	1.217	1.166	1.124
$\ln(\beta/T_p^2)$	-13.593	-12.029	-11.402	-10.744	-10.570
Peak5					
T_p (K)	946.63	967.86	973.33	995.71	1013.08
$1000/T_p$ (K ⁻¹)	1.056	1.033	1.027	1.004	0.987
$\ln(\beta/T_p^2)$	-13.706	-12.141	-11.459	-10.811	-10.623
Peak6					
T_p (K)	1064	1073	1085	1099.13	1115
$1000/T_p$ (K ⁻¹)	0.940	0.932	0.922	0.910	0.897
$\ln(\beta/T_p^2)$	-13.940	-12.347	-11.676	-11.009	-10.814

Table D2 Relation between Heating Rate and Degradation Temperature at Various Conversion for Flynn–Wall–Ozawa method of Peak 1 to Peak 6

Peak1							
β (K/min)		1	5	10	20	25	
$\log \beta$		0.000	0.699	1.000	1.301	1.398	
conversion (%)	10	T (K)	588.22	597.13	605.59	614.84	628.69
		1000/T (K⁻¹)	1.700	1.675	1.651	1.626	1.591
	20	T (K)	594.23	603.54	615.68	624.03	633.81
		1000/T (K⁻¹)	1.683	1.657	1.624	1.602	1.578
	40	T (K)	652.02	661.56	672.69	683.84	698.85
		1000/T (K⁻¹)	1.534	1.512	1.487	1.462	1.431
	60	T (K)	699.36	712.45	723.87	735.09	753.53
		1000/T (K⁻¹)	1.430	1.404	1.381	1.360	1.327
	80	T (K)	713.23	723.06	735.65	751.87	764.87
		1000/T (K⁻¹)	1.402	1.383	1.359	1.330	1.307
	100	T (K)	758.63	769.53	782.67	799.85	815.91
		1000/T (K⁻¹)	1.318	1.299	1.278	1.250	1.226

Table D2 (cont.) Relation between Heating Rate and Degradation Temperature at Various Conversion for Flynn–Wall–Ozawa method of Peak 1 to Peak 6

Peak2							
β (K/min)		1	5	10	20	25	
log β		0.000	0.699	1.000	1.301	1.398	
conversion (%)	10	T (K)	668.51	676.13	688.39	699.45	710.79
		1000/T (K⁻¹)	1.496	1.479	1.453	1.430	1.407
	20	T (K)	685.35	695.63	708.98	717.14	729.97
		1000/T (K⁻¹)	1.459	1.438	1.410	1.394	1.370
	40	T (K)	707.66	717.36	728.58	739.69	753.31
		1000/T (K⁻¹)	1.413	1.394	1.373	1.352	1.327
	60	T (K)	737.33	745.12	754.08	762.34	773.11
		1000/T (K⁻¹)	1.356	1.342	1.326	1.312	1.293
	80	T (K)	762.13	779.85	790.69	802.23	816.25
		1000/T (K⁻¹)	1.312	1.282	1.265	1.247	1.225
	100	T (K)	792.11	806.00	819.00	834.00	846.55
		1000/T (K⁻¹)	1.262	1.241	1.221	1.199	1.181

Table D2 (cont.) Relation between Heating Rate and Degradation Temperature at Various Conversion for Flynn–Wall–Ozawa method of Peak 1 to Peak 6

Peak3							
β (K/min)		1	5	10	20	25	
log β		0.000	0.699	1.000	1.301	1.398	
conversion (%)	10	T (K)	771.93	849.32	895.56	942.13	977.12
		1000/T (K⁻¹)	1.295	1.177	1.117	1.061	1.023
	20	T (K)	796.47	874.15	935.69	975.02	998.56
		1000/T (K⁻¹)	1.256	1.144	1.069	1.026	1.001
	40	T (K)	815.55	896.35	945.58	986.69	1024.56
		1000/T (K⁻¹)	1.226	1.116	1.058	1.013	0.976
	60	T (K)	862.94	906.11	958.69	990.75	1078.09
		1000/T (K⁻¹)	1.159	1.104	1.043	1.009	0.928
	80	T (K)	878.33	916.45	968.58	1019.91	1081.56
		1000/T (K⁻¹)	1.139	1.091	1.032	0.980	0.925
	100	T (K)	901.31	925.69	969.77	1036.06	1086.69
		1000/T (K⁻¹)	1.109	1.080	1.031	0.965	0.920

Table D2 (cont.) Relation between Heating Rate and Degradation Temperature at Various Conversion for Flynn–Wall–Ozawa method of Peak 1 to Peak 6

Peak4							
β (K/min)		1	5	10	20	25	
log β		0.000	0.699	1.000	1.301	1.398	
conversion (%)	10	T (K)	885.03	932.13	945.58	978.69	994.41
		1000/T (K⁻¹)	1.130	1.073	1.058	1.022	1.006
	20	T (K)	907.35	955.32	968.11	996.67	1023.50
		1000/T (K⁻¹)	1.102	1.047	1.033	1.003	0.977
	40	T (K)	944.33	986.22	1009.39	1035.57	1066.89
		1000/T (K⁻¹)	1.059	1.014	0.991	0.966	0.937
	60	T (K)	975.24	1011.65	1041.59	1065.47	1102.02
		1000/T (K⁻¹)	1.025	0.988	0.960	0.939	0.907
	80	T (K)	1012.11	1050.00	1092.00	1103.00	1141.00
		1000/T (K⁻¹)	0.988	0.952	0.916	0.907	0.876
	100	T (K)	1035.33	1072.12	1113.36	1125.95	1167.14
		1000/T (K⁻¹)	0.966	0.933	0.898	0.888	0.857

Table D2 (cont.) Relation between Heating Rate and Degradation Temperature at Various Conversion for Flynn–Wall–Ozawa method of Peak 1 to Peak 6

Peak5							
β (K/min)		1	5	10	20	25	
log β		0.000	0.699	1.000	1.301	1.398	
conversion (%)	10	T (K)	971.03	986.45	1023.69	1034.57	1041.86
		1000/T (K⁻¹)	1.030	1.014	0.977	0.967	0.960
	20	T (K)	977.56	993.38	1028.74	1039.66	1045.66
		1000/T (K⁻¹)	1.023	1.007	0.972	0.962	0.956
	40	T (K)	985.87	1003.03	1037.22	1048.19	1054.13
		1000/T (K⁻¹)	1.014	0.997	0.964	0.954	0.949
	60	T (K)	1015.01	1032.94	1056.32	1078.21	1084.65
		1000/T (K⁻¹)	0.985	0.968	0.947	0.927	0.922
	80	T (K)	1075.55	1099.54	1124.39	1136.11	1158.89
		1000/T (K⁻¹)	0.930	0.909	0.889	0.880	0.863
	100	T (K)	1104.39	1131.11	1156.38	1169.62	1182.22
		1000/T (K⁻¹)	0.905	0.884	0.865	0.855	0.846

Table D2 (cont.) Relation between Heating Rate and Degradation Temperature at Various Conversion for Flynn–Wall–Ozawa method of Peak 1 to Peak 6

Peak6							
β (K/min)		1	5	10	20	25	
log β		0.000	0.699	1.000	1.301	1.398	
conversion (%)	10	T (K)	1065.31	1075.14	1087.69	1099.57	1122.50
		1000/T (K⁻¹)	0.939	0.930	0.919	0.909	0.891
	20	T (K)	1076.44	1085.23	1096.11	1108.89	1131.91
		1000/T (K⁻¹)	0.929	0.921	0.912	0.902	0.883
	40	T (K)	1098.12	1105.95	1119.32	1124.47	1153.35
		1000/T (K⁻¹)	0.911	0.904	0.893	0.889	0.867
	60	T (K)	1122.87	1127.52	1141.13	1146.07	1175.64
		1000/T (K⁻¹)	0.891	0.887	0.876	0.873	0.851
	80	T (K)	1147.13	1149.65	1162.14	1168.36	1198.55
		1000/T (K⁻¹)	0.872	0.870	0.860	0.856	0.834
	100	T (K)	1176.23	1189.11	1201.87	1216.35	1239.03
		1000/T (K⁻¹)	0.850	0.841	0.832	0.822	0.807

Table D3 Relation between Degradation Temperature and Conversion at Various Thermal Mechanism for Coats-Redfern Method of Peak 1 to Peak 6

Peak1							
T (K)	591	594	600	605	607	616	
1000/T (K ⁻¹)	1.692	1.684	1.667	1.653	1.647	1.623	
ln(g(α)/Γ ²)	A2	-14.249	-14.016	-13.869	-13.756	-13.657	-13.596
	A3	-13.754	-13.602	-13.510	-13.441	-13.377	-13.346
	A4	-13.506	-13.395	-13.331	-13.283	-13.237	-13.221
	R1	-15.759	-15.299	-15.001	-14.777	-14.589	-14.456
	R2	-16.440	-15.972	-15.666	-15.433	-15.237	-15.095
	R3	-16.841	-16.371	-16.061	-15.826	-15.627	-15.482
	D1	-18.755	-17.825	-17.208	-16.743	-16.361	-16.065
	D2	-19.431	-18.491	-17.863	-17.387	-16.994	-16.687
	D3	-20.918	-19.967	-19.329	-18.841	-18.437	-18.118
	D4	-20.930	-19.986	-19.355	-18.874	-18.478	-18.166
	F1	-15.734	-15.258	-14.943	-14.702	-14.497	-14.346
	F2	-12.712	-12.690	-12.677	-12.660	-12.631	-12.623
	F3	-12.661	-12.607	-12.561	-12.509	-12.444	-12.400

Table D3 (cont.) Relation between Degradation Temperature and Conversion at Various Thermal Mechanism for Coats-Redfern Method of Peak 1 to Peak 6

		Peak2					
T (K)		687	695	698	703	706	710
1000/T (K ⁻¹)		1.456	1.439	1.433	1.422	1.416	1.408
ln(g(α)/Γ ²)	A2	-14.550	-14.330	-14.171	-14.057	-13.959	-13.880
	A3	-14.055	-13.916	-13.813	-13.741	-13.679	-13.631
	A4	-13.807	-13.709	-13.634	-13.584	-13.539	-13.506
	R1	-16.060	-15.614	-15.304	-15.077	-14.891	-14.740
	R2	-16.741	-16.286	-15.968	-15.733	-15.539	-15.379
	R3	-17.142	-16.685	-16.364	-16.126	-15.929	-15.766
	D1	-19.056	-18.139	-17.511	-17.043	-16.663	-16.349
	D2	-19.732	-18.805	-18.166	-17.687	-17.296	-16.971
	D3	-21.219	-20.281	-19.632	-19.141	-18.739	-18.402
	D4	-21.231	-20.300	-19.657	-19.175	-18.780	-18.451
	F1	-16.035	-15.572	-15.246	-15.002	-14.799	-14.630
	F2	-13.013	-13.004	-12.980	-12.960	-12.933	-12.907
	F3	-12.962	-12.921	-12.863	-12.809	-12.747	-12.684

Table D3 (cont.) Relation between Degradation Temperature and Conversion at Various Thermal Mechanism for Coats-Redfern Method of Peak 1 to Peak 6

		Peak3					
T (K)		821	829	833	835	839	855
1000/T (K ⁻¹)		1.218	1.206	1.200	1.198	1.192	1.170
ln(g(α)/Γ ²)	A2	-14.906	-14.683	-14.525	-14.401	-14.305	-14.252
	A3	-14.411	-14.269	-14.167	-14.085	-14.025	-14.002
	A4	-14.164	-14.062	-13.987	-13.928	-13.884	-13.877
	R1	-16.417	-15.966	-15.657	-15.421	-15.236	-15.112
	R2	-17.097	-16.639	-16.322	-16.077	-15.884	-15.751
	R3	-17.498	-17.037	-16.718	-16.470	-16.274	-16.138
	D1	-19.413	-18.492	-17.865	-17.387	-17.008	-16.721
	D2	-20.089	-19.158	-18.520	-18.031	-17.641	-17.343
	D3	-21.576	-20.634	-19.985	-19.485	-19.084	-18.773
	D4	-21.587	-20.652	-20.011	-19.519	-19.125	-18.822
	F1	-16.391	-15.925	-15.600	-15.347	-15.145	-15.002
	F2	-13.370	-13.357	-13.334	-13.304	-13.278	-13.279
	F3	-13.318	-13.274	-13.217	-13.153	-13.092	-13.056

Table D3 (cont.) Relation between Degradation Temperature and Conversion at Various Thermal Mechanism for Coats-Redfern Method of Peak 1 to Peak 6

		Peak4					
T (K)		969	984	986	987	992	1000
1000/T (K ⁻¹)		1.032	1.016	1.014	1.013	1.008	1.000
ln(g(α)/Γ ²)	A2	-15.238	-15.025	-14.862	-14.735	-14.640	-14.565
	A3	-14.743	-14.611	-14.504	-14.420	-14.360	-14.315
	A4	-14.495	-14.404	-14.325	-14.262	-14.220	-14.190
	R1	-16.748	-16.309	-15.995	-15.755	-15.571	-15.425
	R2	-17.429	-16.981	-16.659	-16.412	-16.219	-16.064
	R3	-17.830	-17.380	-17.055	-16.805	-16.609	-16.451
	D1	-19.744	-18.835	-18.202	-17.722	-17.343	-17.034
	D2	-20.420	-19.500	-18.857	-18.366	-17.976	-17.656
	D3	-21.907	-20.977	-20.322	-19.820	-19.419	-19.087
	D4	-21.919	-20.995	-20.348	-19.853	-19.460	-19.136
	F1	-16.723	-16.268	-15.937	-15.681	-15.480	-15.315
	F2	-13.701	-13.700	-13.671	-13.639	-13.613	-13.592
	F3	-13.650	-13.616	-13.554	-13.488	-13.427	-13.369

Table D3 (cont.) Relation between Degradation Temperature and Conversion at Various Thermal Mechanism for Coats-Redfern Method of Peak 1 to Peak 6

		Peak5					
T (K)		1162	1172	1180	1185	1190	1200
1000/T (K ⁻¹)		0.861	0.853	0.847	0.844	0.840	0.833
ln(g(α)/Γ ²)	A2	-15.601	-15.375	-15.221	-15.101	-15.004	-14.930
	A3	-15.106	-14.961	-14.863	-14.786	-14.723	-14.680
	A4	-14.858	-14.754	-14.684	-14.628	-14.583	-14.555
	R1	-17.112	-16.659	-16.354	-16.121	-15.935	-15.790
	R2	-17.792	-17.331	-17.018	-16.777	-16.583	-16.429
	R3	-18.193	-17.730	-17.414	-17.170	-16.973	-16.816
	D1	-20.107	-19.184	-18.561	-18.087	-17.707	-17.399
	D2	-20.783	-19.850	-19.216	-18.731	-18.340	-18.021
	D3	-22.270	-21.327	-20.682	-20.186	-19.783	-19.451
	D4	-22.282	-21.345	-20.707	-20.219	-19.824	-19.500
	F1	-17.086	-16.617	-16.296	-16.047	-15.844	-15.680
	F2	-14.065	-14.050	-14.030	-14.004	-13.977	-13.957
	F3	-14.013	-13.966	-13.913	-13.853	-13.791	-13.734

Table D3 (cont.) Relation between Degradation Temperature and Conversion at Various Thermal Mechanism for Coats-Redfern Method of Peak 1 to Peak 6

		Peak6					
T (K)		1240	1247	1259	1257	1275	1280
1000/T (K ⁻¹)		0.806	0.802	0.794	0.796	0.784	0.781
ln(g(α)/Γ ²)	A2	-15.731	-15.499	-15.351	-15.219	-15.142	-15.059
	A3	-15.236	-15.085	-14.993	-14.904	-14.861	-14.809
	A4	-14.988	-14.878	-14.814	-14.746	-14.721	-14.684
	R1	-17.241	-16.783	-16.483	-16.239	-16.073	-15.919
	R2	-17.922	-17.455	-17.148	-16.895	-16.721	-16.558
	R3	-18.323	-17.854	-17.544	-17.288	-17.111	-16.945
	D1	-20.237	-19.308	-18.691	-18.205	-17.845	-17.528
	D2	-20.913	-19.974	-19.346	-18.849	-18.478	-18.150
	D3	-22.400	-21.451	-20.811	-20.304	-19.921	-19.580
	D4	-22.412	-21.469	-20.837	-20.337	-19.962	-19.629
	F1	-17.216	-16.741	-16.426	-16.165	-15.982	-15.809
	F2	-14.194	-14.174	-14.160	-14.122	-14.115	-14.086
	F3	-14.143	-14.090	-14.043	-13.971	-13.929	-13.863

Table D4 Conversion and $Z(\alpha)$ Relation at Various Thermal Mechanism according to the Criado Method of Peak 1 to Peak 6

Peak1										
$Z(\alpha)$	α									
	0.0	0.1	0.2	0.3	0.4	0.5	0.6	0.7	0.8	0.9
A2	0.000	0.190	0.357	0.499	0.613	0.693	0.733	0.722	0.644	0.461
A3	0.000	0.284	0.536	0.749	0.919	1.040	1.100	1.084	0.966	0.691
A4	0.000	0.379	0.714	0.999	1.226	1.386	1.466	1.445	1.288	0.921
R1	0.000	0.100	0.200	0.300	0.400	0.500	0.600	0.700	0.800	0.900
R2	0.000	0.097	0.189	0.273	0.349	0.414	0.465	0.495	0.494	0.432
R3	0.000	0.097	0.185	0.265	0.334	0.390	0.429	0.444	0.426	0.346
D1	0.000	0.050	0.100	0.150	0.200	0.250	0.300	0.350	0.400	0.450
D2	0.000	0.049	0.096	0.141	0.183	0.221	0.255	0.281	0.297	0.291
D3	0.000	0.048	0.093	0.133	0.167	0.195	0.214	0.222	0.213	0.173
D4	0.000	0.051	0.102	0.156	0.210	0.267	0.326	0.387	0.450	0.517
F1	0.000	0.095	0.179	0.250	0.306	0.347	0.367	0.361	0.322	0.230
F2	1.000	0.900	0.800	0.700	0.600	0.500	0.400	0.300	0.200	0.100
F3	0.500	0.450	0.400	0.350	0.300	0.250	0.200	0.150	0.100	0.050

Table D4 (cont.) Conversion and $Z(\alpha)$ Relation at Various Thermal Mechanism according to the Criado Method of Peak 1 to Peak 6

Peak2										
$Z(\alpha)$	α									
	0.0	0.1	0.2	0.3	0.4	0.5	0.6	0.7	0.8	0.9
A2	0.000	0.190	0.357	0.499	0.613	0.693	0.733	0.722	0.644	0.461
A3	0.000	0.284	0.536	0.749	0.919	1.040	1.100	1.084	0.966	0.691
A4	0.000	0.379	0.714	0.999	1.226	1.386	1.466	1.445	1.288	0.921
R1	0.000	0.100	0.200	0.300	0.400	0.500	0.600	0.700	0.800	0.900
R2	0.000	0.097	0.189	0.273	0.349	0.414	0.465	0.495	0.494	0.432
R3	0.000	0.097	0.185	0.265	0.334	0.390	0.429	0.444	0.426	0.346
D1	0.000	0.050	0.100	0.150	0.200	0.250	0.300	0.350	0.400	0.450
D2	0.000	0.049	0.096	0.141	0.183	0.221	0.255	0.281	0.297	0.291
D3	0.000	0.048	0.093	0.133	0.167	0.195	0.214	0.222	0.213	0.173
D4	0.000	0.051	0.102	0.156	0.210	0.267	0.326	0.387	0.450	0.517
F1	0.000	0.095	0.179	0.250	0.306	0.347	0.367	0.361	0.322	0.230
F2	1.000	0.900	0.800	0.700	0.600	0.500	0.400	0.300	0.200	0.100
F3	0.500	0.450	0.400	0.350	0.300	0.250	0.200	0.150	0.100	0.050

Table D4 (cont.) Conversion and $Z(\alpha)$ Relation at Various Thermal Mechanism according to the Criado Method of Peak 1 to Peak 6

Peak3										
$Z(\alpha)$	α									
	0.0	0.1	0.2	0.3	0.4	0.5	0.6	0.7	0.8	0.9
A2	0.000	0.190	0.357	0.499	0.613	0.693	0.733	0.722	0.644	0.461
A3	0.000	0.284	0.536	0.749	0.919	1.040	1.100	1.084	0.966	0.691
A4	0.000	0.379	0.714	0.999	1.226	1.386	1.466	1.445	1.288	0.921
R1	0.000	0.100	0.200	0.300	0.400	0.500	0.600	0.700	0.800	0.900
R2	0.000	0.097	0.189	0.273	0.349	0.414	0.465	0.495	0.494	0.432
R3	0.000	0.097	0.185	0.265	0.334	0.390	0.429	0.444	0.426	0.346
D1	0.000	0.050	0.100	0.150	0.200	0.250	0.300	0.350	0.400	0.450
D2	0.000	0.049	0.096	0.141	0.183	0.221	0.255	0.281	0.297	0.291
D3	0.000	0.048	0.093	0.133	0.167	0.195	0.214	0.222	0.213	0.173
D4	0.000	0.051	0.102	0.156	0.210	0.267	0.326	0.387	0.450	0.517
F1	0.000	0.095	0.179	0.250	0.306	0.347	0.367	0.361	0.322	0.230
F2	1.000	0.900	0.800	0.700	0.600	0.500	0.400	0.300	0.200	0.100
F3	0.500	0.450	0.400	0.350	0.300	0.250	0.200	0.150	0.100	0.050

Table D4 (cont.) Conversion and $Z(\alpha)$ Relation at Various Thermal Mechanism according to the Criado Method of Peak 1 to Peak 6

Peak4										
$Z(\alpha)$	α									
	0.0	0.1	0.2	0.3	0.4	0.5	0.6	0.7	0.8	0.9
A2	0.000	0.190	0.357	0.499	0.613	0.693	0.733	0.722	0.644	0.461
A3	0.000	0.284	0.536	0.749	0.919	1.040	1.100	1.084	0.966	0.691
A4	0.000	0.379	0.714	0.999	1.226	1.386	1.466	1.445	1.288	0.921
R1	0.000	0.100	0.200	0.300	0.400	0.500	0.600	0.700	0.800	0.900
R2	0.000	0.097	0.189	0.273	0.349	0.414	0.465	0.495	0.494	0.432
R3	0.000	0.097	0.185	0.265	0.334	0.390	0.429	0.444	0.426	0.346
D1	0.000	0.050	0.100	0.150	0.200	0.250	0.300	0.350	0.400	0.450
D2	0.000	0.049	0.096	0.141	0.183	0.221	0.255	0.281	0.297	0.291
D3	0.000	0.048	0.093	0.133	0.167	0.195	0.214	0.222	0.213	0.173
D4	0.000	0.051	0.102	0.156	0.210	0.267	0.326	0.387	0.450	0.517
F1	0.000	0.095	0.179	0.250	0.306	0.347	0.367	0.361	0.322	0.230
F2	1.000	0.900	0.800	0.700	0.600	0.500	0.400	0.300	0.200	0.100
F3	0.500	0.450	0.400	0.350	0.300	0.250	0.200	0.150	0.100	0.050

Table D4 (cont.) Conversion and $Z(\alpha)$ Relation at Various Thermal Mechanism according to the Criado Method of Peak 1 to Peak 6

Peak5										
$Z(\alpha)$	α									
	0.0	0.1	0.2	0.3	0.4	0.5	0.6	0.7	0.8	0.9
A2	0.000	0.190	0.357	0.499	0.613	0.693	0.733	0.722	0.644	0.461
A3	0.000	0.284	0.536	0.749	0.919	1.040	1.100	1.084	0.966	0.691
A4	0.000	0.379	0.714	0.999	1.226	1.386	1.466	1.445	1.288	0.921
R1	0.000	0.100	0.200	0.300	0.400	0.500	0.600	0.700	0.800	0.900
R2	0.000	0.097	0.189	0.273	0.349	0.414	0.465	0.495	0.494	0.432
R3	0.000	0.097	0.185	0.265	0.334	0.390	0.429	0.444	0.426	0.346
D1	0.000	0.050	0.100	0.150	0.200	0.250	0.300	0.350	0.400	0.450
D2	0.000	0.049	0.096	0.141	0.183	0.221	0.255	0.281	0.297	0.291
D3	0.000	0.048	0.093	0.133	0.167	0.195	0.214	0.222	0.213	0.173
D4	0.000	0.051	0.102	0.156	0.210	0.267	0.326	0.387	0.450	0.517
F1	0.000	0.095	0.179	0.250	0.306	0.347	0.367	0.361	0.322	0.230
F2	1.000	0.900	0.800	0.700	0.600	0.500	0.400	0.300	0.200	0.100
F3	0.500	0.450	0.400	0.350	0.300	0.250	0.200	0.150	0.100	0.050

Table D4 (cont.) Conversion and $Z(\alpha)$ Relation at Various Thermal Mechanism according to the Criado Method of Peak 1 to Peak 6

Peak6										
$Z(\alpha)$	α									
	0.0	0.1	0.2	0.3	0.4	0.5	0.6	0.7	0.8	0.9
A2	0.000	0.190	0.357	0.499	0.613	0.693	0.733	0.722	0.644	0.461
A3	0.000	0.284	0.536	0.749	0.919	1.040	1.100	1.084	0.966	0.691
A4	0.000	0.379	0.714	0.999	1.226	1.386	1.466	1.445	1.288	0.921
R1	0.000	0.100	0.200	0.300	0.400	0.500	0.600	0.700	0.800	0.900
R2	0.000	0.097	0.189	0.273	0.349	0.414	0.465	0.495	0.494	0.432
R3	0.000	0.097	0.185	0.265	0.334	0.390	0.429	0.444	0.426	0.346
D1	0.000	0.050	0.100	0.150	0.200	0.250	0.300	0.350	0.400	0.450
D2	0.000	0.049	0.096	0.141	0.183	0.221	0.255	0.281	0.297	0.291
D3	0.000	0.048	0.093	0.133	0.167	0.195	0.214	0.222	0.213	0.173
D4	0.000	0.051	0.102	0.156	0.210	0.267	0.326	0.387	0.450	0.517
F1	0.000	0.095	0.179	0.250	0.306	0.347	0.367	0.361	0.322	0.230
F2	1.000	0.900	0.800	0.700	0.600	0.500	0.400	0.300	0.200	0.100
F3	0.500	0.450	0.400	0.350	0.300	0.250	0.200	0.150	0.100	0.050

APPENDIX E

Kinetic Parameters Reported in Literature

Table E1 Kinetic Parameters and Thermal Degradation Mechanism Reported in Other Literature.

Peak	T _p (°C)	E _a (kJ/mol)				Mechanism		
		KS	FWO	CR	Other	CR	Criado	Other
1	397	248	241	244	220 [14]	F1	F1	F1 [14]
2	454	281	288	289	240 [14]	F1	F1	F1 [14]
3	526	232	219	222	130-170 [76]	F1	F1	D3 [76]
4	584	115	107	103	80-100 [78]	F1	F1	F1 [78]
5	722	365	362	345	330 [75]	F1	F1	F1 [75]
6	827	523	531	525	480-520 [77]	F1	F1	NA

REFERENCES

1. Kchaou, M., Sellami, A., Elleuch, R., and Singh, H., Friction characteristics of a brake friction material under different braking conditions. *Materials & Design* (1980-2015), 2013. **52**: p. 533-540.
2. Friedrich, K., Polymer composites for tribological applications. *Advanced Industrial and Engineering Polymer Research*, 2018. **1**(1): p. 3-39.
3. Guarino, V., Gentile, G., Sorrentino, L., and Ambrosio, L., *Encyclopedia of Polymer Science and Technology*. 2017, John Wiley & Sons, Inc.
4. Takeichi, T., Kawauchi, T., and Agag, T., High performance polybenzoxazines as a novel type of phenolic resin. *Polymer journal*, 2008. **40**(12): p. 1121-1131.
5. Cai, P., Wang, Y., Wang, T., and Wang, Q., Effect of resins on thermal, mechanical and tribological properties of friction materials. *Tribology International*, 2015. **87**: p. 1-10.
6. Chan, D. and Stachowiak, G., Review of automotive brake friction materials. *Proceedings of the Institution of Mechanical Engineers, Part D: Journal of Automobile Engineering*, 2004. **218**(9): p. 953-966.
7. Ghosh, N., Kiskan, B., and Yagci, Y., Polybenzoxazines—new high performance thermosetting resins: synthesis and properties. *Progress in polymer Science*, 2007. **32**(11): p. 1344-1391.
8. Ishida, H. and Agag, T., *Handbook of benzoxazine resins*. 2011: Elsevier.
9. Nair, C.R., Advances in addition-cure phenolic resins. *Progress in polymer science*, 2004. **29**(5): p. 401-498.
10. Wirasate, S., Dhumrongvaraporn, S., Allen, D.J., and Ishida, H., Molecular origin of unusual physical and mechanical properties in novel phenolic materials based on benzoxazine chemistry. *Journal of applied polymer science*, 1998. **70**(7): p. 1299-1306.
11. Kim, H. and Ishida, H., Model compounds study on the network structure of polybenzoxazines. *Macromolecules*, 2003. **36**(22): p. 8320-8329.
12. Ishida, H. and Allen, D.J., Gelation behavior of near zero shrinkage polybenzoxazines. *Journal of applied polymer science*, 2001. **79**(3): p. 406-417.
13. Ishida, H. and Allen, D.J., Physical and mechanical characterization of near zero

- shrinkage polybenzoxazines. *Journal of polymer science Part B: Polymer physics*, 1996. **34**(6): p. 1019-1030.
14. Tiptipakorn, S., Damrongsakkul, S., Ando, S., Hemvichian, K., and Rimdusit, S., Thermal degradation behaviors of polybenzoxazine and silicon-containing polyimide blends. *Polymer degradation and stability*, 2007. **92**(7): p. 1265-1278.
15. Kragel'skii, I.V. and Mikhin, N.M., *Handbook of friction units of machines*. 1988: Amer Society of Mechanical.
16. Dante, R.C., *Handbook of friction materials and their applications*. 2015: Woodhead Publishing.
17. Ludema, K.C. and Ajayi, O.O., *Friction, wear, lubrication: a textbook in tribology*. 2018: CRC press.
18. Day, A., *Braking of Road Vehicles*. 2014: Elsevier Inc.
19. Orthwein, W.C., *Clutches and brakes: design and selection*. 2004: CRC Press.
20. Mahmoud, K.R.M., *Theoretical and experimental investigations on a new adaptive duo servo drum brake with high and constant brake shoe factor*. 2005: HNI.
21. Automotive, C., *Fundamentals of Automotive Technology: Principles and Practice*. 2013: Jones & Bartlett Publishers.
22. Dante, R., *Handbook of Friction Materials and their Applications*. 1 ed. 2016: Woodhead Publishing in Materials.
23. Sturmeay, H. and Staner, H.W., *The Autocar: A Journal Published in the Interests of the Mechanically Propelled Road Carriage*. Vol. 134. 1971: Iliffe, sons & Sturmeay Limited.
24. Hutchings, I. and Shipway, P., *Tribology: friction and wear of engineering materials*. 2017: Butterworth-Heinemann.
25. Bely, V., Sviridenok, A., and Petrokovets, M., *Friction and wear in polymer-based materials*. 2013: Elsevier.
26. Ishida, H. and Froimowicz, P., *Advanced and emerging polybenzoxazine science and technology*. 2017: Elsevier.
27. Gurunath, P.V. and Bijwe, J., *Friction and wear studies on brake-pad materials based on newly developed resin*. 16th International Conference on Wear of Materials, 2017. **263**.

28. Ning, X. and Ishida, H., Phenolic materials via ring opening polymerization: Synthesis and characterization of bisphenol: A based benzoxazines and their polymers. *Journal of Polymer Science Part A: Polymer Chemistry*, 1994. **32**(6).
29. Thorpe, A. and Harrison, R.M., Sources and properties of non-exhaust particulate matter from road traffic: a review. *Science of the total environment*, 2008. **400**(1-3): p. 270-282.
30. Eriksson, M., Bergman, F., and Jacobson, S., On the nature of tribological contact in automotive brakes. *Wear*, 2002. **252**(1-2): p. 26-36.
31. Kumar, M. and Bijwe, J., Role of different metallic fillers in non-asbestos organic (NAO) friction composites for controlling sensitivity of coefficient of friction to load and speed. *Tribology International*, 2010. **43**(5-6): p. 965-974.
32. Wenbin, L., Jianfeng, H., Jie, F., Zhenhai, L., Liyun, C., and Chunyan, Y., Effect of aramid pulp on improving mechanical and wet tribological properties of carbon fabric/phenolic composites. *Tribology International*, 2016. **104**: p. 237-246.
33. Li, J., The effect of carbon fiber content on the mechanical and tribological properties of carbon fiber-reinforced PTFE composites. *Polymer-Plastics Technology and Engineering*, 2010. **49**(4): p. 332-336.
34. Sampath, V., Studies on mechanical, friction, and wear characteristics of Kevlar and glass fiber-reinforced friction materials. *Materials and manufacturing processes*, 2006. **21**(1): p. 47-57.
35. Ma, Y., Wu, S., Tong, J., Zhao, X., Zhuang, J., Liu, Y., and Qi, H., Tribological and mechanical behaviours of rattan-fibre-reinforced friction materials under dry sliding conditions. *Materials Research Express*, 2018. **5**(3): p. 035101.
36. Kumar, M. and Bijwe, J., Non-asbestos organic (NAO) friction composites: role of copper; its shape and amount. *Wear*, 2011. **270**(3-4): p. 269-280.
37. Jang, H. and Kim, S.J., The effects of antimony trisulfide (Sb₂S₃) and zirconium silicate (ZrSiO₄) in the automotive brake friction material on friction characteristics. *Wear*, 2000. **239**(2): p. 229-236.
38. Holly, F.W. and Cope, A.C., Condensation products of aldehydes and ketones with o-aminobenzyl alcohol and o-hydroxybenzylamine. *Journal of the American Chemical Society*, 1944. **66**(11): p. 1875-1879.

39. Burke, W., 3, 4-Dihydro-1, 3, 2H-Benzoxazines. Reaction of p-substituted phenols with N, N-dimethylolamines. *Journal of the American Chemical Society*, 1949. **71**(2): p. 609-612.
40. Burke, W. and Stephens, C.W., Monomeric products from the condensation of phenol with formaldehyde and primary amines. *Journal of the American Chemical Society*, 1952. **74**(6): p. 1518-1520.
41. Wypych, G., *Handbook of polymers*. 2016: Elsevier.
42. Ishida, H. and Sanders, D.P., Improved thermal and mechanical properties of polybenzoxazines based on alkyl substituted aromatic amines. *Journal of Polymer Science Part B: Polymer Physics*, 2000. **38**(24).
43. Ishida, H. and Allen, D.J., Physical and mechanical characterization of near zero shrinkage polybenzoxazines. *Journal of polymer science Part B: Polymer physics*, 1996. **34**(6).
44. Ishida, H. and Rodriguez, Y., Curing kinetics of a new benzoxazine-based phenolic resin by differential scanning calorimetry. *polymer*, 1995. **36**(16): p. 3151-3158.
45. Rimdusit, S., Kunopast, P., and Dueramae, I., Thermomechanical properties of arylamine-based benzoxazine resins alloyed with epoxy resin. *Polymer Engineering & Science*, 2011. **51**(9): p. 1797-1807.
46. Al-Salem, S., *Plastics to energy: fuel, chemicals, and sustainability implications*. 2018: William Andrew.
47. Dahiya, J.B., Kumar, K., Muller-Hagedorn, M., and Bockhorn, H., Kinetics of isothermal and non isothermal degradation of cellulose: model based and model free methods. *Polymer International*, 2008. **57**(5).
48. Vyazovkin, S., Chrissafis, K., Di Lorenzo, M.L., Koga, N., Pijolat, M., Roduit, B., Sbirrazzuoli, N., and Suñol, J.J., ICTAC Kinetics Committee recommendations for collecting experimental thermal analysis data for kinetic computations. *Thermochimica acta*, 2014. **590**: p. 1-23.
49. Balart, R., Garcia-Sanoguera, D., Quiles-Carrillo, L., Montanes, N., and Torres-Giner, S., Kinetic analysis of the thermal degradation of recycled acrylonitrile-butadiene-styrene by non-isothermal thermogravimetry. *Polymers*, 2019. **11**(2): p. 281.
50. Vyazovkin, S., Kissinger method in kinetics of materials: Things to beware and be

aware of. *Molecules*, 2020. **25**(12): p. 2813.

51. Kissinger, H.E., Reaction kinetics in differential thermal analysis. *Analytical chemistry*, 1957. **29**(11): p. 1702-1706.

52. Ozawa, T., A new method of analyzing thermogravimetric data. *Bulletin of the chemical society of Japan*, 1965. **38**(11): p. 1881-1886.

53. Coats, A.W. and Redfern, J., Kinetic parameters from thermogravimetric data. *Nature*, 1964. **201**(4914): p. 68-69.

54. Nam, J.d. and Seferis, J.C., A composite methodology for multistage degradation of polymers. *Journal of Polymer Science Part B: Polymer Physics*, 1991. **29**(5): p. 601-608.

55. Elmay, Y., Jeguirim, M., Trouvé, G., and Said, R., Kinetic analysis of thermal decomposition of date palm residues using Coats–Redfern method. *Energy Sources, Part A: Recovery, Utilization, and Environmental Effects*, 2016. **38**(8): p. 1117-1124.

56. Cai, J. and Bi, L., Precision of the Coats and Redfern method for the determination of the activation energy without neglecting the low-temperature end of the temperature integral. *Energy & Fuels*, 2008. **22**(4): p. 2172-2174.

57. Criado, J.M. and Pérez-Maqueda, L.A., The accuracy of Senum and Yang's approximations to the Arrhenius integral. *Journal of Thermal Analysis and Calorimetry*, 2000.

58. Criado, J.M., Malek, J., and Ortega, A., Applicability of the master plots in kinetic analysis of a non-isothermal rate. *Thermochimica Acta*, 1989.

59. Paterson, W.L., Computation of the exponential trap population integral of glow curve theory. *Journal of Computational Physics*, 1971. **7**(1): p. 187-190.

60. Urbanovici, E., Popescu, C., and Segal, E., Improved iterative version of the Coats-Redfern method to evaluate non-isothermal kinetic parameters. *Journal of Thermal Analysis and Calorimetry*, 1999. **58**(3): p. 683-700.

61. Perejón, A., Sánchez-Jiménez, P.E., Criado, J.M., and Pérez-Maqueda, L.A., Kinetic analysis of complex solid-state reactions. A new deconvolution procedure. *The journal of physical chemistry B*, 2011. **115**(8): p. 1780-1791.

62. Sharma, P., Pandey, O., and Diwan, P., Non-isothermal kinetics of pseudo-components of waste biomass. *Fuel*, 2019. **253**: p. 1149-1161.

63. Kurihara, S., Idei, H., Aoyagi, Y., Kuroe, M., Binder Resin for Friction Material. U.S.

Patent 8,227,390 B2. 2012.

64. Wu, Y., Zeng, M., Xu, Q., Hou, S., Jin, H., and Fan, L., Effects of glass-to-rubber transition of thermosetting resin matrix on the friction and wear properties of friction materials. *Tribology International*, 2012. **54**: p. 51-57.
65. Ishida, H. and Sanders, D.P., Regioselectivity and network structure of difunctional alkyl-substituted aromatic amine-based polybenzoxazines. *Macromolecules*, 2000. **33**(22): p. 8149-8157.
66. Rimdusit, S., Thamprasom, N., Suppakarn, N., Jubsilp, C., Takeichi, T., and Tiptipakorn, S., Effect of triphenyl phosphate flame retardant on properties of arylamine-based polybenzoxazines. *Journal of Applied Polymer Science*, 2013. **130**(2): p. 1074-1083.
67. Low, H.Y. and Ishida, H., Mechanistic study on the thermal decomposition of polybenzoxazines: effects of aliphatic amines. *Journal of Polymer Science Part B: Polymer Physics*, 1998. **36**(11): p. 1935-1946.
68. Valliyappan, N., Berhan, D., Darius, M., and Solomon, G., Thermal characteristics of novel brake friction materials for light rail transit applications. *WIT Transactions on the Built Environment*, 2006. **88**: p. 167-176.
69. Jubsilp, C., Takeichi, T., and Rimdusit, S., Property enhancement of polybenzoxazine modified with dianhydride. *Polymer degradation and stability*, 2011. **96**(6): p. 1047-1053.
70. Dueramae, I., Jubsilp, C., Takeichi, T., and Rimdusit, S., Thermal degradation mechanism of highly filled nano-SiO₂ and polybenzoxazine. *Journal of Thermal Analysis and Calorimetry*, 2014. **116**(1): p. 435-446.
71. Jubsilp, C., Jantaramaha, J., Mora, P., and Rimdusit, S., Tribological Performance and Thermal Stability of Nanorubber-Modified Polybenzoxazine Composites for Non-Asbestos Friction Materials. *Polymers*, 2021. **13**(15): p. 2435.
72. Wongpayakyotin, A., Jubsilp, C., Tiptipakorn, S., Mora, P., Bielawski, C.W., and Rimdusit, S., Effects of Alkyl-Substituted Polybenzoxazines on Tribological Properties of Non-Asbestos Composite Friction Materials. *Polymers*, 2021. **13**(4): p. 567.
73. Landel, R.F. and Nielsen, L.E., Mechanical properties of polymers and composites. 1993: CRC press.

74. Ran, Q.c., Tian, Q., Li, C., and Gu, Y., Investigation of processing, thermal, and mechanical properties of a new composite matrix benzoxazine containing aldehyde group. *Polymers for Advanced Technologies*, 2010. **21**(3).
75. Hemvichian, K. and Ishida, H., Thermal decomposition processes in aromatic amine-based polybenzoxazines investigated by TGA and GC-MS. *Polymer*, 2002. **43**(16): p. 4391-4402.
76. Lertwassana, W., Parnklang, T., Mora, P., Jubsilp, C., and Rimdusit, S., High performance aramid pulp/carbon fiber-reinforced polybenzoxazine composites as friction materials. *Composites Part B: Engineering*, 2019. **177**: p. 107-280.
77. Li, X.G. and Huang, M.R., Thermal degradation of Kevlar fiber by high-resolution thermogravimetry. *Journal of applied polymer science*, 1999. **71**(4): p. 565-571.
78. Tsamba, A.J., Yang, W., and Blasiak, W. Cashew nut shells char reactivity and combustion kinetics. in 26th Annual International Conference on Incineration and Thermal Treatment Technologies, IT3, 14 May 2007 through 18 May 2007, Phoenix, AZ, United States. 2007.
79. Mohazzabi, P. and Searcy, A.W., Kinetics and thermodynamics of decomposition of barium sulphate. *Journal of the Chemical Society, Faraday Transactions 1: Physical Chemistry in Condensed Phases*, 1976. **72**: p. 290-295.
80. Mayasari, H., Setyorini, I., and Yuniari, A. Thermal degradation and swelling behaviour of acrylonitrile butadiene styrene rubber reinforced by carbon black. in IOP Conference Series: Materials Science and Engineering. 2018. IOP Publishing.
81. Koleva, D., Atanassov, A., and Nedelchev, N., Nonisothermal degradation kinetics of ultra-high molecular weight polyethylene composites filled with carbon or aramid fibers. *International Journal of Polymeric Materials*, 2008. **57**(9): p. 841-851.
82. Moguet, F., Bordère, S., Tressaud, A., Rouquerol, F., and Llewellyn, P., Deintercalation process of fluorinated carbon fibres—II. Kinetic study and reaction mechanisms. *Carbon*, 1998. **36**(7-8): p. 1199-1205.



จุฬาลงกรณ์มหาวิทยาลัย
CHULALONGKORN UNIVERSITY

VITA

NAME Juntasak Wangrangsimakul

DATE OF BIRTH 1 October 1984

PLACE OF BIRTH Surathani, Thailand

INSTITUTIONS ATTENDED B.Eng. Chemical Engineering
King Mongkut's Institute of Technology Ladkrabang

HOME ADDRESS 16-18 Chonvitee Road, T. Talad, A. Mueng, Surathani,
Thailand



จุฬาลงกรณ์มหาวิทยาลัย
CHULALONGKORN UNIVERSITY